Journal of Natural Gas Science and Engineering 51 (2018) 166–182

Contents lists available at ScienceDirect

Journal of Natural Gas Science and Engineering

journal homepage: www.elsevier.com/locate/jngse

Diagenesis of microbialites in the lower Cambrian Qingxudong Formation, South China: Implications for the origin of porosity in deep microbial carbonates

Qian Tan[a,b], Zejin Shi[a,b,*], XiuQuan Hu[b], Yong Wang[c], YaMing Tian[c], ChangCheng Wang[b]

[a] State Key Laboratory of Oil and Gas Reservoir Geology and Exploitation, Chengdu University of Technology, Chengdu 610059, China
[b] College of Energy Resources, Chengdu University of Technology, Chengdu 610059, China
[c] College of Earth Sciences, Chengdu University of Technology, Chengdu 610059, China

ARTICLE INFO

Keywords:
Microbial carbonate
Diagenesis
Porosity origin
Dolomitization and dissolution
Sichuan basin

ABSTRACT

Understanding microbial carbonate is one of the most challenging issues in the field of carbonate sedimentology and reservoir. The biotic and abiotic processes that control microbial carbonate precipitation are becoming more established, but the influence of subsequent diagenesis on microbial carbonate reservoirs has not been adequately studied. Here, we describe microbial carbonate from the lower Cambrian Qingxudong Formation in southeastern Sichuan Basin to assess their formation, textures and subsequent diagenesis. Six stages of calcite cementation (Calcite-1 to Calcite-6) and four stages of dissolution (Dis-1 to Dis-4) were identified in microbialites of the Qingxudong Formation. Stromatolites and thrombolites have a different porosity evolution. Sedimentary processes are the fundamental controlling factors of creating pre-existing pores in stromatolites. For thrombolites, the formation of pre-existing pores is attributed to island dissolution and dolomitization in near-surface processes. Microbial metabolic activities contribute more to the dissolution and dolomitization than mixing water. Meteoric water dissolution (Dis-1) in synsedimentary processes and microbial dissolution (Dis-2) in near-surface processes are the fundamental control factors of porosity creation in microbial carbonate of Qingxudong Formation. Thermochemical sulfate reduction (TSR) is a double-edged sword for the porosity development. The destructive effect of TSR on microbial carbonate reservoirs is greater than the constructive effect. The microbial carbonate reservoirs, especially the fabric-destructive dolomite (Dol-2) evolved by thrombolites, have great potential for gas exploration in the Qingxudong Formation. This study is especially useful for further understanding deeply buried microbialite reservoir formation and development, and deep hydrocarbon exploration in this basin and elsewhere worldwide.

1. Introduction

Microbial processes that are involved in the formation, mineralization, accumulation and diagenesis of carbonate sediments are regarded as one of the most popular topics in the field of carbonate sedimentology and geochemistry (Riding, 2000; Flügel, 2004; Aloisi, 2008; Shiraishi et al., 2008; Dupraz et al., 2009; Mercedes-Martín et al., 2014; Hips et al., 2015; Tan et al., 2017). Biological, abiotic and environmental factors controlling microbial carbonate precipitation and these processes resulting in a variety of textures and fabrics, which provide a template for microbial carbonate (microbialite) reservoir porosity and permeability (Parcell, 2002; Al Haddad and Mancini, 2013; Mancini et al., 2013; Rezende et al., 2013; Słowakiewicz et al., 2013; Pederson et al., 2015). However, the influence of diagenetic processes on deeply buried microbial carbonate reservoirs has not been adequately studied.

Deeply buried microbial carbonate rocks have been tightly cemented and compacted by postdepositional deposits (Shi et al., 2013; Słowakiewicz et al., 2013; Song et al., 2014) and thus may not be qualified as reservoirs. However, three types of diagenetic stages (eogenetic, mesogenetic, and telogenetic dissolution) have been proposed that lead to the dissolution of carbonates, original organic matter and sulfates and improve porosity and permeability in carbonate reservoirs (Vacher and Mylroie, 2002; Flügel, 2004; Zhu et al., 2006; Li et al., 2016; Zhang et al., 2017). Eogenetic dissolution (karst) occurs in exposed coastal or island carbonate settings that have not been subjected to burial and diagenesis (Vacher and Mylroie, 2002; Menning et al., 2015). The secondary pores may have been created by meteoric water

* Corresponding author. State Key Laboratory of Oil and Gas Reservoir Geology and Exploitation, Chengdu University of Technology, Chengdu 610059, China.
E-mail address: szj@cdut.edu.cn (Z. Shi).

https://doi.org/10.1016/j.jngse.2017.12.031
Received 1 September 2017; Received in revised form 8 December 2017; Accepted 29 December 2017
Available online 12 January 2018
1875-5100/

(Raeisi and Mylroie, 1995; Zhang et al., 2017), the mixing of fresh and saline waters (Back et al., 1986; Vacher and Mylroie, 2002; Mylroie and Mylroie, 2007; Menning et al., 2015) and CO_2 from the degradation of organic matter (Machel, 2001; Gulley et al., 2013, 2014). Mesogenetic (burial) dissolution occurs in middle to late-burial settings where fluids that are charged with organic acids, such as CO_2 and H_2S that occur from the maturation of organic matter and thermochemical sulfate reduction (TSR) related to hydrothermal activity could create significant dissolution (Esteban and Taberner, 2003; Lambert et al., 2006; Zhu et al., 2006). Some authors had debated that burial dissolution has little contribution to porosity enhancement (Ehrenberg et al., 2012; Zhang et al., 2017) and some emphasized that TSR had an overall destructive effect on carbonate reservoirs (Hao et al., 2015). Therefore, the generation of secondary porosity still remains controversial in carbonates and is less understood in deep-burial microbial carbonates.

The lower Cambrian Qingxudong (Longwangmiao) Formation in the Sichuan Basin has been a primary target for hydrocarbon exploration for several decades, which has recently made significant achievements (Jin et al., 2014; Zhou et al., 2014; Zou et al., 2014). The deposition and diagenesis and their controls on porosity, in the reservoirs have been intensively studied (e.g. Mei et al., 2006; Li et al., 2012; Jin et al., 2014; Zhou et al., 2014; Zou et al., 2014), but controversy regarding the deposition and the generation of secondary porosity still remains. The reservoirs mainly consist of grain shoal facies in the central Sichuan Basin (Jin et al., 2014; Zhou et al., 2014; Zou et al., 2014), but the reservoirs mainly consist of microbial reef-shoals in the southeastern Sichuan Basin (Hicks and Rowland, 2009; Li et al., 2012; Adachi et al., 2014; Ren et al., 2016). Some scholars have emphasized that the secondary porosity was generated by dissolution from meteoric water during the telogenetic diagenesis stage (Jin et al., 2014; Yang et al., 2015). However, some have also stressed the input of subaerial exposure and attendant dissolution by meteoric or mixing water in the eogenetic stage (Li et al., 2012; Zhou et al., 2014). Further, some have proposed that the secondary porosity were generated by deep-burial dissolution including hydrothermal dissolution (Tian et al., 2014). These controversies indicate that the porosity formation related to diagenetic processes has not been adequately studied.

In attempt to answer this controversial issue, the main objective of this paper, therefore, is to (1) characterize the Qingxudong Formation microbial carbonates of the southeastern Sichuan Basin, focusing on their external and internal features and providing insights into the model for microbial carbonate reservoirs; (2) analyse the diagenetic components of microbialites which reveals the temporal and spatial succession of diagenetic processes including marine processes, eogenetic processes and mesogenetic processes; and (3) discuss the origin and evolution of porosity according to the diagenetic components and reservoir characteristics of the microbialites. The results provide guidance for further oil and gas exploration in the region, and advance our understanding of the genesis of microbial carbonate reservoirs.

2. Geologic setting

The southeastern Sichuan Basin is located in the middle-upper Yangtze region, mainly including Sichuan and Guizhou Provinces and Chongqing City (Fig. 1). The basin was developed during the tectonic modification movement of basement rocks, the breakup of peripheral basement blocks and basin filling (Zhou et al., 2014; Zou et al., 2014). During deposition of the lower Cambrian Qingxudong Formation, which was influenced by basement tectonic movement and block breakup, a narrow slope that transitioned into a deep-water basin was formed near the Dayong fault (Steiner et al., 2005). As a result, the basin and its periphery as a whole were covered by shallow platform deposits during the Qingxudong period (Fig. 1). Although the Sichuan Basin was filled by the Qiongzhusi and Canglangpu Formations in the early Cambrian, it still maintained a palaeogeographic setting that was characterized by alternating grabens and horsts that were inclined from northwest to the southeast as a whole (Zhou et al., 2014). According to the palaeogeographic reconstructions, the Sichuan Basin and its periphery were located around the palaeoequator in the Cambrian period, with a warm and humid palaeoclimate (Scotese, 2001). The palaeogeomorphy and palaeoclimate determined the distribution of sedimentary microfacies, in which grain banks and interbank deposits developed in the Central Sichuan Paleo-uplift to the west of the Huayingshan fault, evaporative tidal flat and evaporative lagoons formed between the Huayingshan fault and the Qiyueshan fault, and intra-platform micobial reef-banks and interbank deposits formed along the Qiyueshan fault and the Dayong fault (Fig. 1).

The Qingxudong Formation was named for the Qingxudong limestone in the Meitan County of the Guizhou Province, as a part of *Hoffetella- Pteroredlichiamurakamii* and *Redlichianobilistrilobites* zone, and is age-equivalent to the Longwangmiaoan stage in China (Li et al., 2012). Since the Sichuan Basin and its periphery had different provenances, sedimentary environments, palaeogeomorphy, palaeontology and tectonic background during deposition of the Cambrian strata, the basin has benn divided into multiple stratigraphic zones (Li et al., 2012). In the Early Cambrian, the Yangtze platform was covered extensively by archaeocyathid reef-banks, but archaeocyathids were replaced by microbialites during deposition of the lower Cambrian Qingxudong Formation (Fig. 2, Hicks and Rowland, 2009; Adachi et al., 2014).

In the study area, the Qingxudong Formation is mainly composed of limestone, dolomitic limestone and dolomite, with an average thickness of about 200 m (Fig. 3). It can easily be separated from clastic strata in the underlying Jindingshan Formation and overlying Gaotai Formation (Li et al., 2012). The Qingxudong Formation is divided into two third-order transgressive–regressive (T-R) sequences (Fig. 3, Mei et al., 2006; Li et al., 2012), and the T-R sequence is composed of a transgressive systems tract (TST) and a regressive systems tract (RST, Fig. 3). In the first transgressive–regressive sequence (T-R sequence 1) period, a restricted platform and an open platform developed and were characterized by a dominance of thrombolites. In the second transgressive–regressive sequence (T-R sequence 2) period, the evaporative tidal flats developed and were characterized by a dominance of stromatolites.

3. Evaluation of samples and methods

Field identification of the lithologies mainly relied on a hand lens and 5% HCl. Lithologies were further identified in the lab by analysis of thin sections. The microscopic features of microbialites were largely determined based on optical microscope examination. Freshly broken sample fragments were analyzed using a FEI Quanta FEG 250, and the micro-zone elemental composition was analyzed using energy disperse spectroscopy (EDS, Oxford INCAx max20) at the State Key Laboratory of Oil and Gas Reservoir Geology and Exploitation, Chengdu University of Technology, Chengdu, China.

Carbon/oxygen isotope compositional analyses was completed in the Geochemistry Laboratory of the Chengdu University of Technology, with a MAT252 isotope radio mass spectrometer equipped with dual inlet systems at a temperature of 22 °C and humidity of 50% respectively. During the sample preparation, in order to avoid the influence of mineral impurity, fresh samples were first selected, and then representative samples that were drilled out with micro-drills were ground with an agate mortar to 200 mesh and placed in the oven for drying. Later, the powder was reacted with 100% H_3PO_4 to extract CO_2 for isotopic testing. The PDB criterion was used for calculating millesimal error of the data, and the analysis precision was ± 0.2‰.

Sr isotope tests were completed in the State Key Laboratory of Oil and Gas Reservoir Geology and Exploitation, Chengdu University of Technology. After 50 mg samples of 200 mesh were dissolved by dilute acetic acid and HCl and dried on a heating plate, additional HCl solution was added for dissolution of samples (Huang et al., 2002). Then

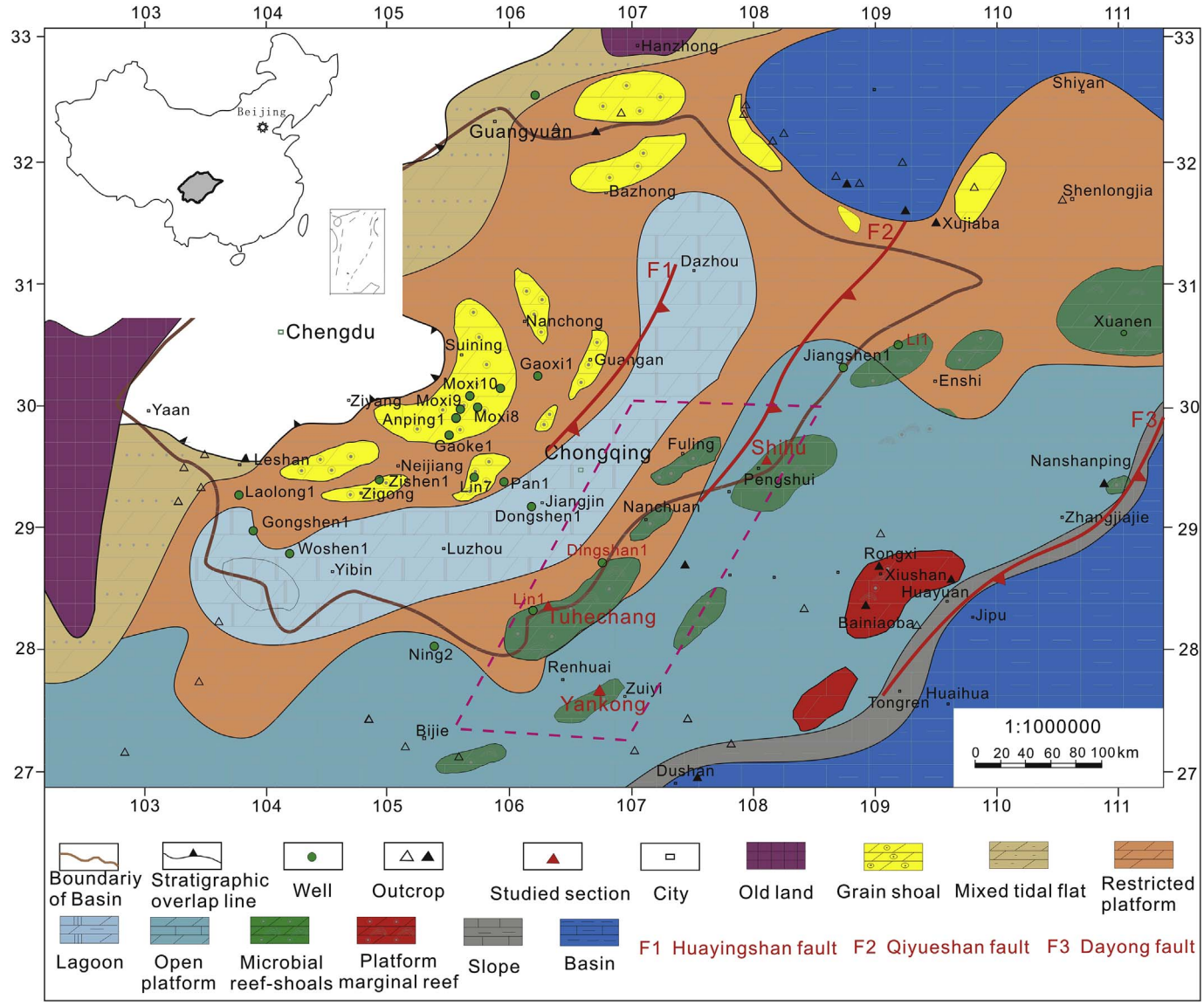

Fig. 1. Lithofacies palaeogeography of the lower Cambrian Qingxudong Formation in the Sichuan Basin, illustrating the distribution of sedimentary facies and the microbial reef-banks in southeastern Sichuan Basin (dotted line), and the sampling locations (red triangles). (For interpretation of the references to colour in this figure legend, the reader is referred to the Web version of this article.)

1 ml liquor was used to isolate pure Sr on an AG50WX8 cation-exchange resin column after centrifugation. Finally, Sr isotopes were measured with a MAT-261 isotope radio mass spectrometer. According to the repeated tests on standard Sr sample NBS987, the $^{87}Sr/^{86}Sr$ value was defined as (0.710283 ± 0.000045), with a measurement error less than 0.01%.

Thin sections were observed with cathodoluminescence under operation conditions of 300 mA and 5 kV and images were collected after evacuation in 10s exposure in the laboratory in the College of Energy Resources, Chengdu University of Technology. Mn and Sr content measurements was completed with an ICP-MS to assess the influence of diagenesis on microcrystalline limestone.

4. Petrography

4.1. Stromatolites

4.1.1. Macrostructure

Stratiform stromatolites are the most common buildups in the study area and mainly occur in T-R sequence 2 (Fig. 3). Stratiform stromatolites are composed of vertically stacked, flat-to undulating laminated beds, with thickness that vary greatly between 80 and 150 cm, locally reaching 270 cm (Fig. 4A). Horizontally, their shape and thickness change slightly, and the thicker part expands widely. Vertically, the foundations for growth of the stromatolites are thick dolarenite and/or oolitic dolomite banks (Fig. 3). In some cases, small conical (with heights and widths up to 45 cm and 25 cm, respectively) or cylindrical (with diameters and heights up to 35 cm and 45 cm, respectively) rock structures are visible at the bottom of the stratiform stromatolites (Fig. 4B). The internal structures of the biostromes are dominated by smooth, continuous, flat rhythmic lamination, as well as undulating lamination (Fig. 4C and D). Flat laminae coexist with or continuously alternate with wavy laminae (Fig. 4C). Undulating laminae are wavy, and some even present obvious wave-like curves (Fig. 4D). In some cases, dendritic structures are observed in the top of stratiform stromatolites, with heights of 10–30 cm and diameters of 2–4 cm (Fig. 4D). Laminae of stromatolites, especially stratiform stromatolites, are alternate as dark to bright colours. Bright laminae are usually thicker than the dark ones. In addition, domal stromatolites locally overlie the stratiform stromatolites (Fig. 4E).

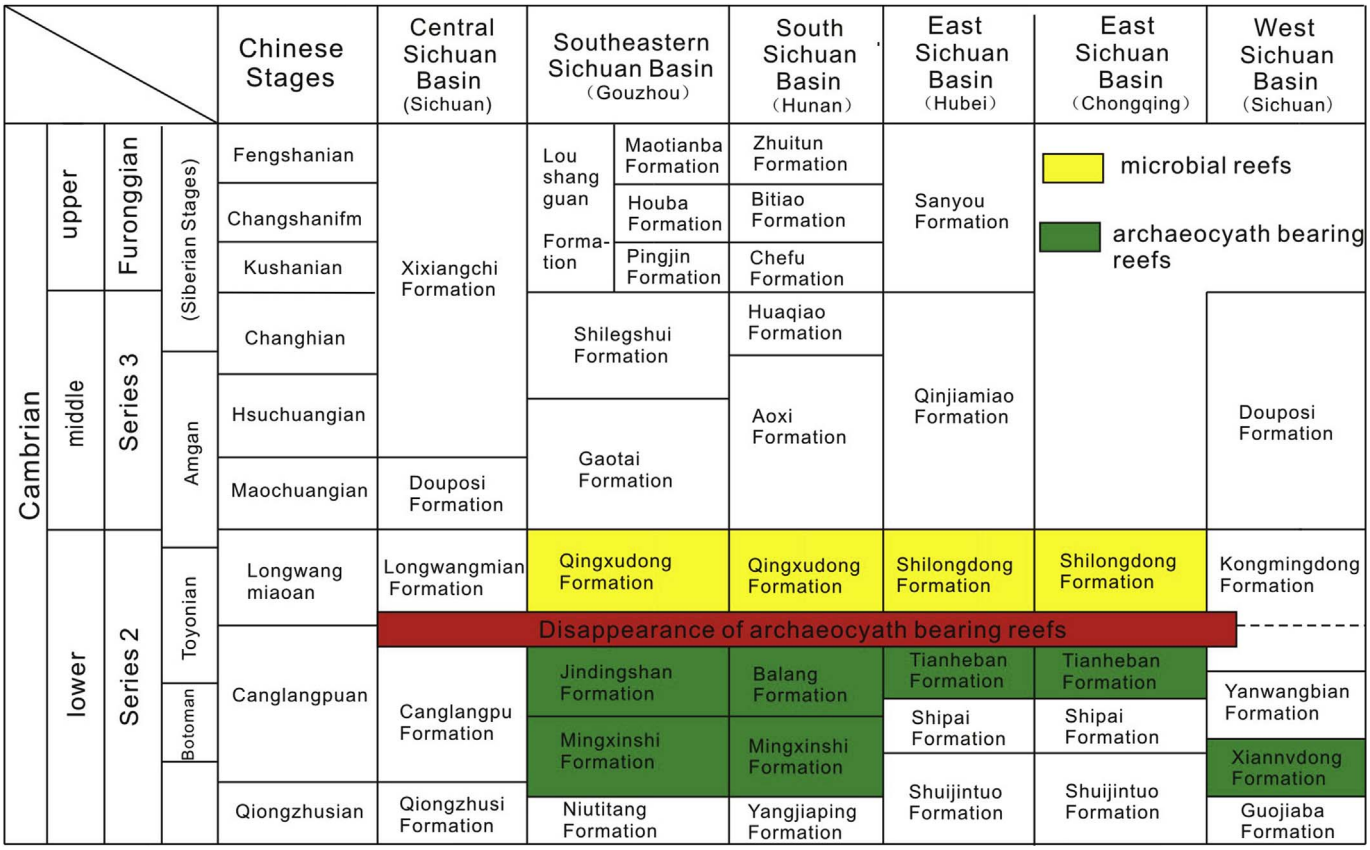

Fig. 2. Distribution of early Cambrian reefs, chronostratigraphic subdivisions and correlations with Siberian subdivisions (modified after Adachi et al., 2014).

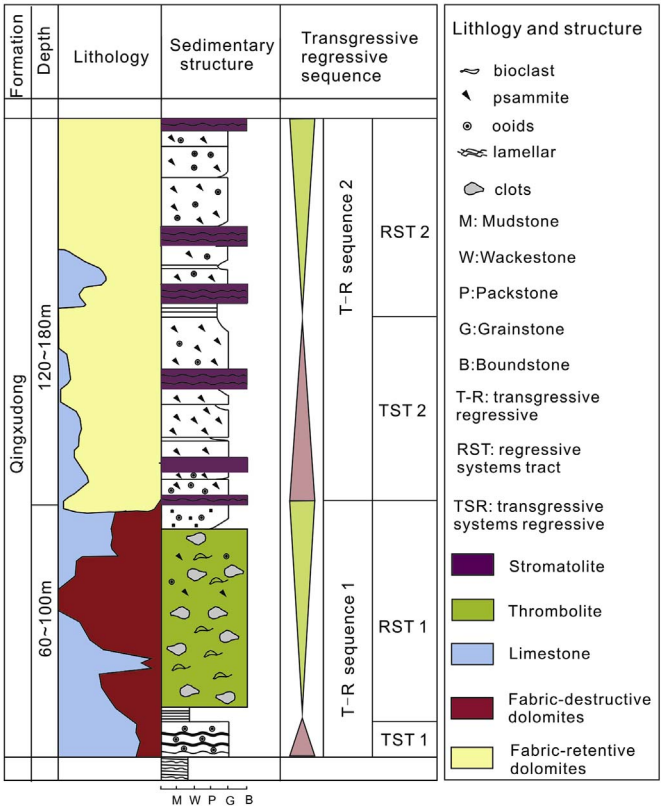

Fig. 3. Lithostratigraphic column and the sequence stratigraphic framework of the early Cambrian Qingxudong Formation in this study.

4.1.2. *Microstructure*

The stromatolites characterized by fabric-retentive microcrystalline dolomites (Dol-1) that mostly consist of bright and dark, planar to subplanar or crinkly laminae (Fig. 5A–D). Dark laminae are mainly composed of dense microcrystalline dolomite and microbial remains (Fig. 5E and F). Some small quartz grains are occasionally embedded (Fig. 5C). Single dark laminae are generally 0.1–1.2 mm thick, with a flat to domal cross-section (Fig. 5A–E). Bright laminae are mainly composed of neomorphic, euhedral to subhedral dolomicrosparite, peloidal dolomicrite and less calcite (Fig. 5E and F). Single bright laminations are generally 0.25–3 mm thick, with a flat to domal cross-section (Fig. 5A–E). Fenestral pores exist and are partly filled by sparry calcite cements (Fig. 5E). Microbial trace fossils (Possibly *Girvanella*) or parallel and vertical microbial filaments are mixed to form a chaotic network (Fig. 5E). The micron-sized (400–800 nm in diameter) spheroidal bodies (Fig. 5F) are interpreted as mineralized bacteria or original synsedimentary bacterial forms (possibly spores, Perri and Tucker, 2007). The fibrous texture bodies (aragonite, Fig. 5F) are likely the brackets that prevented movement of the spheroidal bodies. The spheroidal bodies likely protect microbes from the adverse environmental conditions.

4.1.3. *Interpretation*

The dolarenite and/or oolitic dolomite banks associated with the stromatolites (Fig. 3) support a shallow water environment (Flügel, 2004). The absence of grain deposits in stromatolites (Figs. 4 and 5) indicates a low-energy environment. The birdeye structures (Fig. 4D), desiccation cracks (Fig. 5D) and low-diversity of bioclasts link to evaporation in arid conditions (Flügel, 2004; Dupraz et al., 2009; Mercedes-Martín et al., 2014). Thus, these stromatolites form in a low-energy tidal flat environment with high evaporation. The formation condition of stromatolite is favorable for transitory subaerial exposure in synsedimentary stage (Flügel, 2004). Moreover, arid conditions and

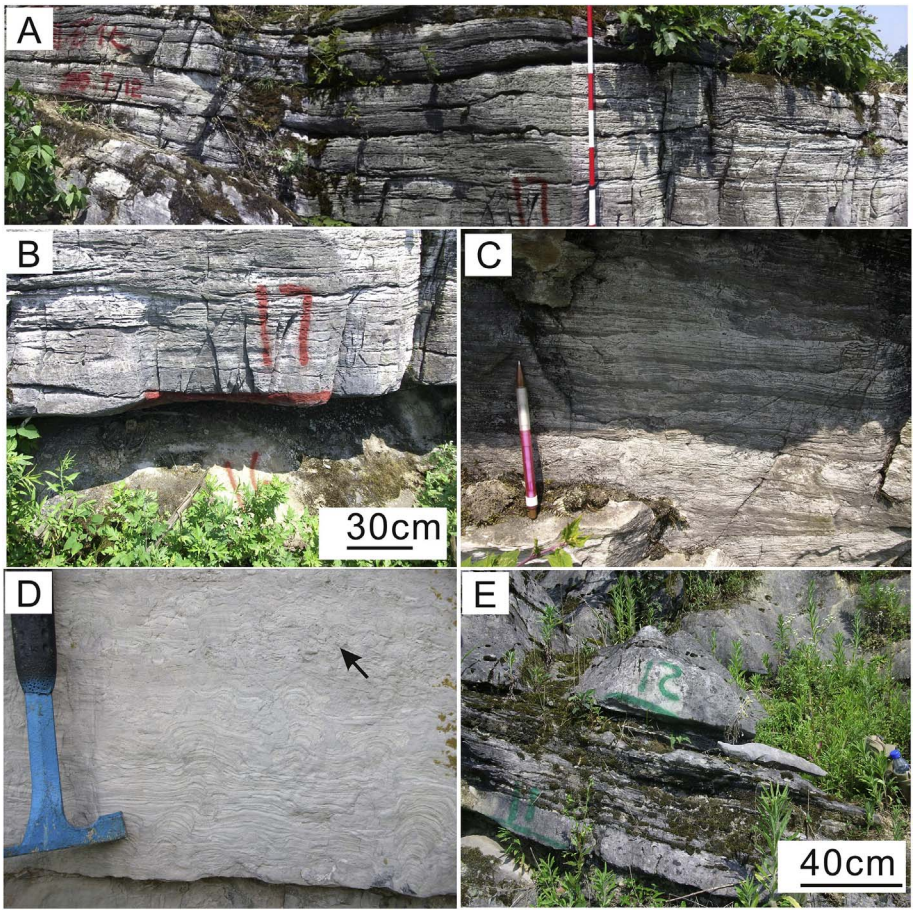

Fig. 4. Macrostructure of stromatolites. (A) Stratiform stromatolite. (B) Partial enlargement of the bottom of A, showing small conic and cylindrical structures. (C) Partial enlargement of the middle of A, with bright and dark laminaes. (D) Dendritic structures in the top of stratiform stromatolite, with acicular solution pores (dark arrow). (E) Domal stromatolite above a stratiform stromatolite. The colour scale of ruler, pencil and hammer are 20 cm, 14 cm and 32 cm long, respectively. (For interpretation of the references to colour in this figure legend, the reader is referred to the Web version of this article.)

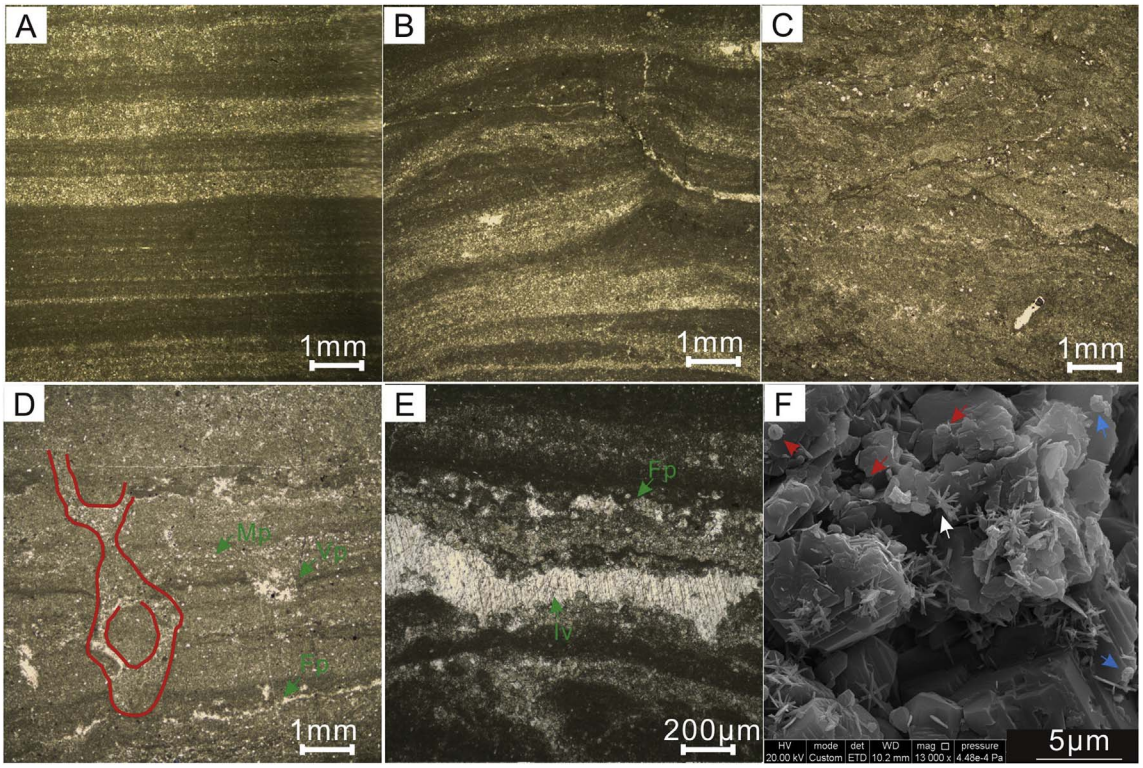

Fig. 5. Microstructure of stromatolites. (A) Flat bright-dark alternating laminae. (B) Wavy bright-dark alternating laminae. (C) Microstructure of dendritic stromatolite, showing disordered laminae with alternating bright-dark colours. (D) Sparry laminae with pelletoid structures in stromatolite with desiccation cracks (red solid line), fenestral porosity (Fp), mouldic porosity (Mp) and vuggy porosity (Vp). (E) The interlaminar void (Iv) in a stromatolite. (F) Spheroidal structured bodies (red arrows), fibrous textured bodies (white arrow) and bacteria (blue arrows) are enclosed within dolomite crystals. (For interpretation of the references to colour in this figure legend, the reader is referred to the Web version of this article.)

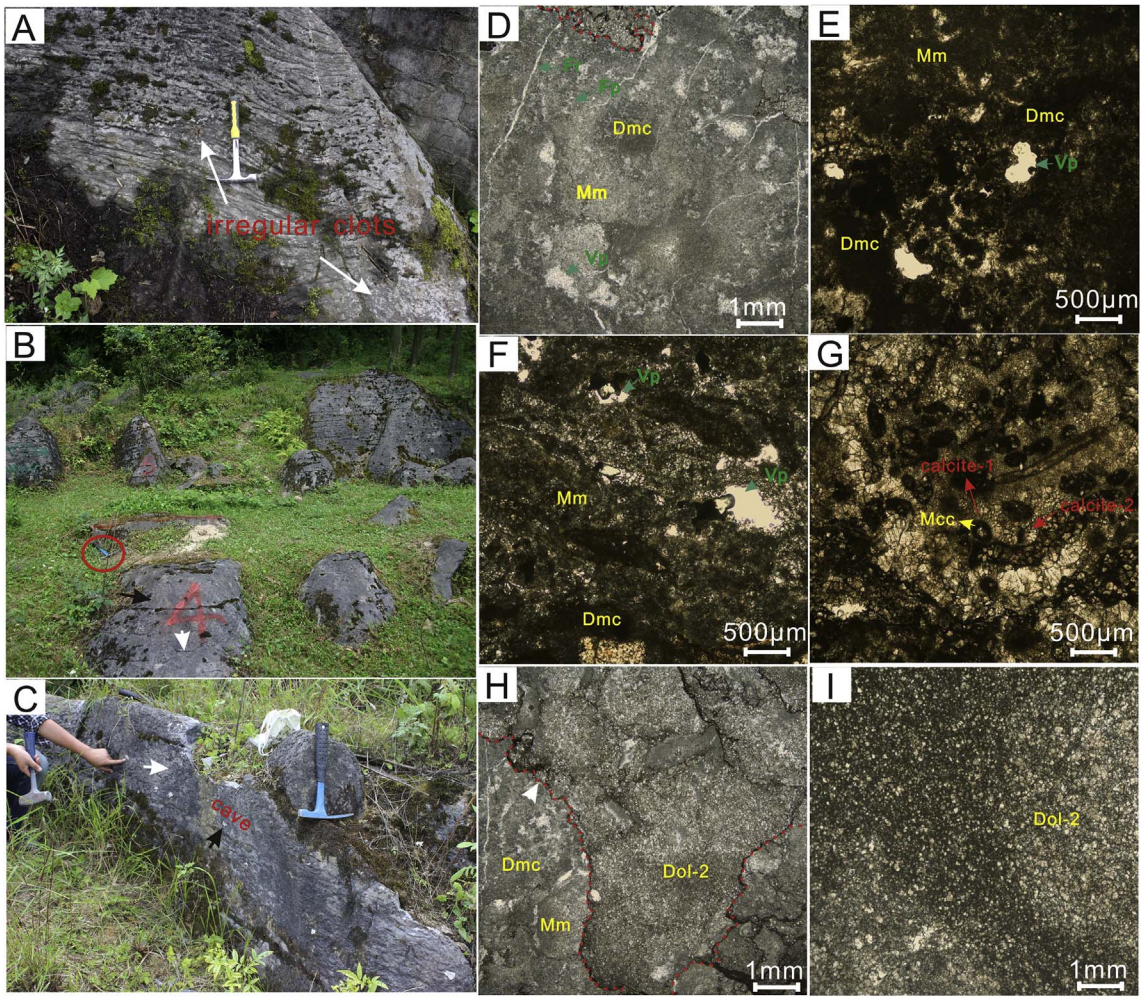

Fig. 6. Macrostructure and microstructure of thrombolites; Dmc = dense micritic clots; Mm = micritic matrix; fabric-destructive-dolomite = Dol-2; fibrous cements = Calcite-1; granular cements = Calcite-2. (A) Stratiform structure with porphyritic clots. (B) Domal structure with thrombolitic textures. (C) Stratiform and domal structures, with strips and nets of clots and solution pores filled by calcite. (D) Common thrombolitic texture. Dmc is composed by microbes and related mud. Mm is composed of a homogeneous light mudstone that represents the internal sediment. (E), (F) Dmc is composed of dark-colored and massive microcrystalline masses. Microbial bodies are rounded and filamentous in shape, which likely represent coccoid bacteria and *Girvanella* groups. (G) Intraclasts and peloids encrusted by biofilms and fabric-selective dolomitization developing in clots. (H) Dol-2 in the thrombolite. Note that Dol-2 is filling the interframework cavity that was likely generated by corrosion processes (dashed line). (I) Dol-2 (fabric-destructive dolomite) with a graniphyric texture.

microbial metabolic activities are beneficial for dissolvable mineral deposition including evaporite minerals, aragonite and high Mg-calcite (Fig. 5F, Dupraz et al., 2009; Brauchli et al., 2016).

4.2. Thrombolites

4.2.1. Macrostructure

Thrombolites with a clotted fabric occur mainly in the lower part of T-R sequence 1 (Fig. 3), and are dominantly characterized by domal structures and stratiform structures (Fig. 6A–C). The stratiform thrombolites are as thick as several meters (Fig. 6A). Domal thrombolites vary remarkably in size from a few tens of centimeters to 2–3 m in width and height (Fig. 6B). Domal thrombolites are in tangent and intersected contact, or exist as isolated single bioherms (Fig. 6B). The clotted fabric in both domal and stratiform thrombolites consists generally of black or dark grey irregular clots, with shapes included subrounded, arborescent, ellipsoidal, and crescent-shaped, with clear boundaries and sizes ranging from 0.2 to 4.5 cm (Fig. 6A and B). In some cases, some clots form continuous or discontinuous strips (Fig. 6C). Thrombolites in the Qingxudong Formation can be divided into two classes: Class A, includes thrombolite mounds that are interbedded with bioclastic limestone and micritic limestone, are dominated by limestone, and show selective dolomitization; and Class B includes thrombolite reefs that are interbedded with oolitic limestone, calcarenite and bioclastic limestone, and show extensive dolomitization. In addition, the grain contents of Class B thrombolites are markedly increased.

4.2.2. Microstructure

Thrombolites are composed of a clotted texture and are commonly constituted by dense micritic clots, micritic matrix and cements (Fig. 6D–G). The dense micritic clots (Dmc) represent the prime microbial constituents and are characterized by dark-colored, dense microcrystalline masses that are arborescent, sub-rounded and crescent-shaped (Fig. 6D–G). These clots are commonly composed of dispersed and aggregated microbial bodies (e.g. arborescent, coccoid and filamentous bacteria) and surrounding mud (Fig. 6D–G). In some cases, intraclastics and/orpeloids that are encrusted by calcified biofilms (Fig. 6G). The micritic matrix (Mm) between the Dmc consists of homogeneous light mudstone and less wackestone that is composed of intraclasts and peloidals (Fig. 6D–F). The clots, intraclasts and peloidals are occasionally wrapped in microbial crusts (Mcc). Some samples, especially in the Class B thrombolites, contain abundant fibrous and botryoidal cements (Fig. 6G) that can constitute 20%–40% of volume of some thin-sections.

Fabric-selective dolomitization and non-fabric-selective

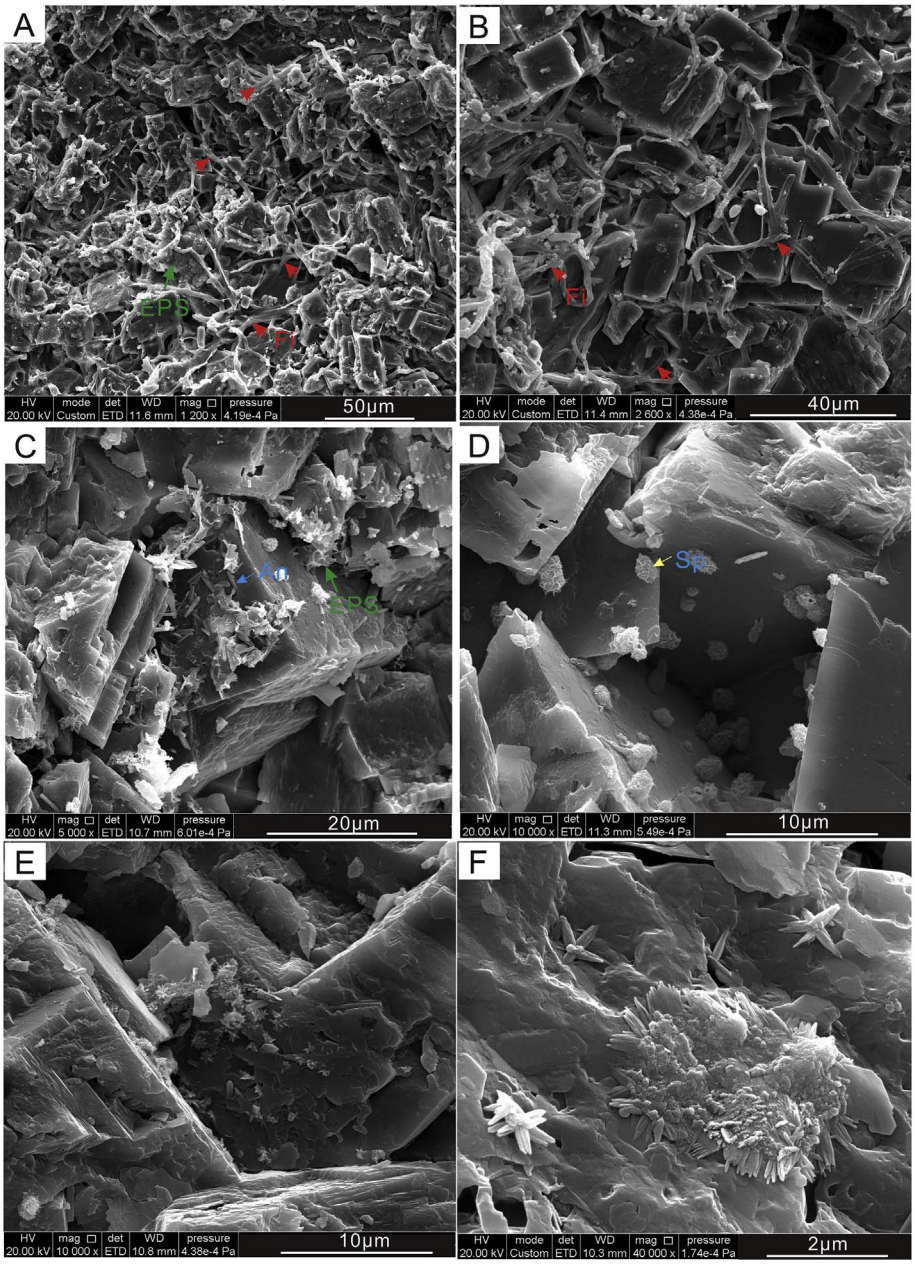

Fig. 7. Scanning electron microscope (SEM) micrographs of neomorphic dolomite with microbial textures in the thrombolites. (A) Micrograph showing microbial filaments and extracellular polymeric substances (EPSs) with granular-textured surfaces enclosed within dolomite crystals. (B) Micrograph showing microbial filaments draped over crystals. (C) Aragonite needles and degradation of EPS. (D) Spheroids associated with EPS within the inter-crystalline space. (E), (F) Aragonite with radial textures protruding from surfaces of dolomite and EPS.

dolomitization are universal in the thrombolites. The dolomitized thrombolites are marked by fabric-destructive dolomites (Dol-2). Fabric-selective dolomitization usually develops in Dmc, intraclasts and peloids (Fig. 6G). Non-fabric-selective dolomitization usually develops in irregularly elongated cavities (Fig. 6H). There is evidence of neomorphic, euhedral to subhedral dolomicrosparite to dolosparite that shows a piebald structure and replaces the dense micritic clots and micritic matrix. In some areas, the thrombolites are entirely replaced with Dol-2 (Fig. 6I).

SEM microscopy shows that dolomite spar that varies from 15 to 80 μm in size is wrapped by filamentous substances and EPS (extracellular polymeric substances) with granular-textured surfaces (Fig. 7A and B). The filamentous substances and EPS are commonly interpreted as microbial in origin and the granular-textured surfaces have often been interpreted to represent mineralized ultramicrobacteria or decomposition, dehydration and shrinkage of micron-sized bacterial forms (Perri and Tucker, 2007; Dupraz et al., 2009). Needle-like crystals of authigenic aragonite (~10 μm in long) are enclosed within dolomite crystals and EPS (Fig. 7C). Spheroidal structures with 0.5–2 μm in diameter occur between crystals within the intercrystalline pore space (Fig. 7D). Aragonites with fibrous textures occur on surfaces of dolomite crystals (Fig. E, F). The aragonites associated with EPS are likely to have an organic origin, especially the degradation of EPS (Hover et al., 2001; Brauchli et al., 2016). The spheroidal bodies have been interpreted as original synsedimentary spores (Perri and Tucker, 2007).

4.2.3. Interpretation

The accumulation of the micritic matrix (Mm, Fig. 6D, F) indicates a low-energy subtidal environment. However, the grain deposits (Fig. 6G and H) and clotted textures indicate a higher energy shallow condition. The abundant bioclastics (Fig. 6H) and fibrous and botryoidal cements (Fig. 6H) indicate a relatively open shallow condition. Thus, a shallow subtidal open marine environment is proposed for the formation of the thrombolites.

Thrombolites were partly dolomitized and the dolomites are characterized by fabric-destructive textures. Similar dolomites were suggested for the Jurassic Smackover Formation thrombolites in Mexico (Mancini et al., 2013). The dolomites wrapped by filamentous and EPSs

Table 1
Symbols of different stages of calcite cementation.

	Petrographic features	Cathodeluminescence features	Carbon, oxygen isotopes	Strontium isotopes	Diagenesis environment	
Calcite-1	fibrous cements forming isopachous grain coatings	nonluminescence	δ13C: 0.37‰–0.84‰; δ18O: −8.13‰ ~ −8.40‰	0.70954–0.70981	marine origin	marine environment and/or eogenetic environmen
Calcite-2	granular cements distributing between microbial clots					
Calcite-3	blocky cements with variously sized crystals	bright orange luminescence	δ13C: −2.46‰ ~ −3.25‰; δ18O: −8.24‰ ~ −10.33‰	0.70986–0.71265	meteoric origin	eogenetic environmen
Calcite-4	syntaxial cements showing clean crystal surface	nonluminescence	–	–	marine origin	shallow burial environmen
Calcite-5	coarse-crystal blocky	weak luminescence	δ13C: 0.56‰–0.65‰; δ18O: −9.21‰ ~ −9.67‰	0.70928–0.70944		deep burial environmen
Calcite-6	granular and coarse-crystal cements	dull red luminescence	δ13C: −6.03‰ ~-29.64‰; δ18O: −9.59‰ ~ −10.13‰	0.70997–0.71374	hydrothermal fluids origin	

(extracellular polymeric substances) with granular-textured surfaces (Fig. 7A and B). The widespread EPS with granular-textured surfaces (nanometer-sized spheres) suggest bacterial degradation of original organic matter (Perri and Tucker, 2007). The processes of EPS degradation (Fig. 7A, C) are particularly significant in dolomite precipitation (Dupraz et al., 2009; Perri and Tucker, 2007; Bontognali et al., 2010; Hips et al., 2015), indicating microbes and EPS played a significant role in the formation of the dolomites. Aragonite precipitation (Fig. 7E and F) is favorable for pore formation in eogenetic processes (Zhang et al., 2017).

4.3. Calcite cementation

According to the morphology of calcite crystals and petrological features that are highlighted by the cathodoluminescence response of the calcite crystals, six types of calcite cementation that critically impact the reservoir quality are identified. The petrographic descriptions of calcite cements are provided (Table 1).

Four types of early or syn-sedimentary cements are recognized: fibrous cements and granular cements (Calcite-1) that are characterized by isopachous crusts (Fig. 8A and B) that are distributed between microbial clots; botryoidal and foliated cements (Calcite-2) with hackly crusts (Fig. 8C and D); blocky cements (Calcite-3) with variably sized crystals (Fig. 8E–H); and syntaxial cements (Calcite-4) with clean crystal surfaces (Fig. 8I and J). Under cathodoluminescence (CL), Calcite-1 (Fig. 8B) and Calcite-2 (Fig. 8B, D) display a general non-luminescence that is occasionally dotted with orange spots and rims. Calcite-4 is non-luminescent (Fig. 8H). Calcite-3 has a bright orange luminescence (Fig. 8F, H). The petrological features of Calcite-1, Calcite-2 and Calcite-4 are commonly interpreted as a marine origin and the Calcite-3 has a meteoric origin (Flügel, 2004; Shi et al., 2013). Early fractures (Ef) are currently cut by large pores and late fractures (Lf) commonly passed through the cementation of pores (Fig. 8E–H).

Two types of burial cements are observed: coarse-crystalline blocky cements (Calcite-5, Fig. 8A) and mosaic and/or coarse-crystal cements (Calcite-6, Fig. 8K and L) that are characterized by pore-filling calcite crystals. Calcite-5 has weak luminescence with orange rims under CL (Fig. 8B) and Calcite-6 has a weak luminescence or a non-luminescence (Fig. 8K and L). In addition, the dolomite cements have orange or dull reddish luminescence and authigenic quartz has a non-luminescence filled in pores and fractures (Fig. 8M–P). The dissolved saddle dolomite remnants suspended in the Calcite-6 (Fig. 8 M, N), indicating a remarkable dissolution after the dolomite formation. The petrological features of Calcite-5 and Calcite-6 are commonly interpreted as a burial origin and a TRS origin, respectively (Flügel, 2004; Shi et al., 2013).

5. Reservoir characteristics of microbialites

5.1. Types of porosity in microbialites

Observations from thin sections show that fenestral porosity, shelter porosity, mouldic porosity, vuggy porosity, caves and fractures are the major pore types in the microbialites reservoirs of the Qingxudong Formation. Ancient porosity, especially primary porosity, in microbialites that appears in thin sections appears to be occluded by sparry calcite cements and less commonly by dolomite and quartz cements. Most of the open porosity has a weathering origin.

Fenestral (Fig. 5B, E) and shelter porosity (Fig. 6D) of variable sizes and shapes ranges from micrometres to millimetres wide and occurs within microbial laminae and clots. The porosity is enlarged by early to late dissolution processes to become interlaminar voids (Fig. 5E) and vuggy porosity (Figs. 5D and 6D) that are currently occluded by sparry calcite cements.

Vuggy porosity and caves tend to be the most common open pores and widely distributed in the microbialites of the Qingxudong Formation (Figs. 5 and 6). Most vuggy porosity and caves present well-

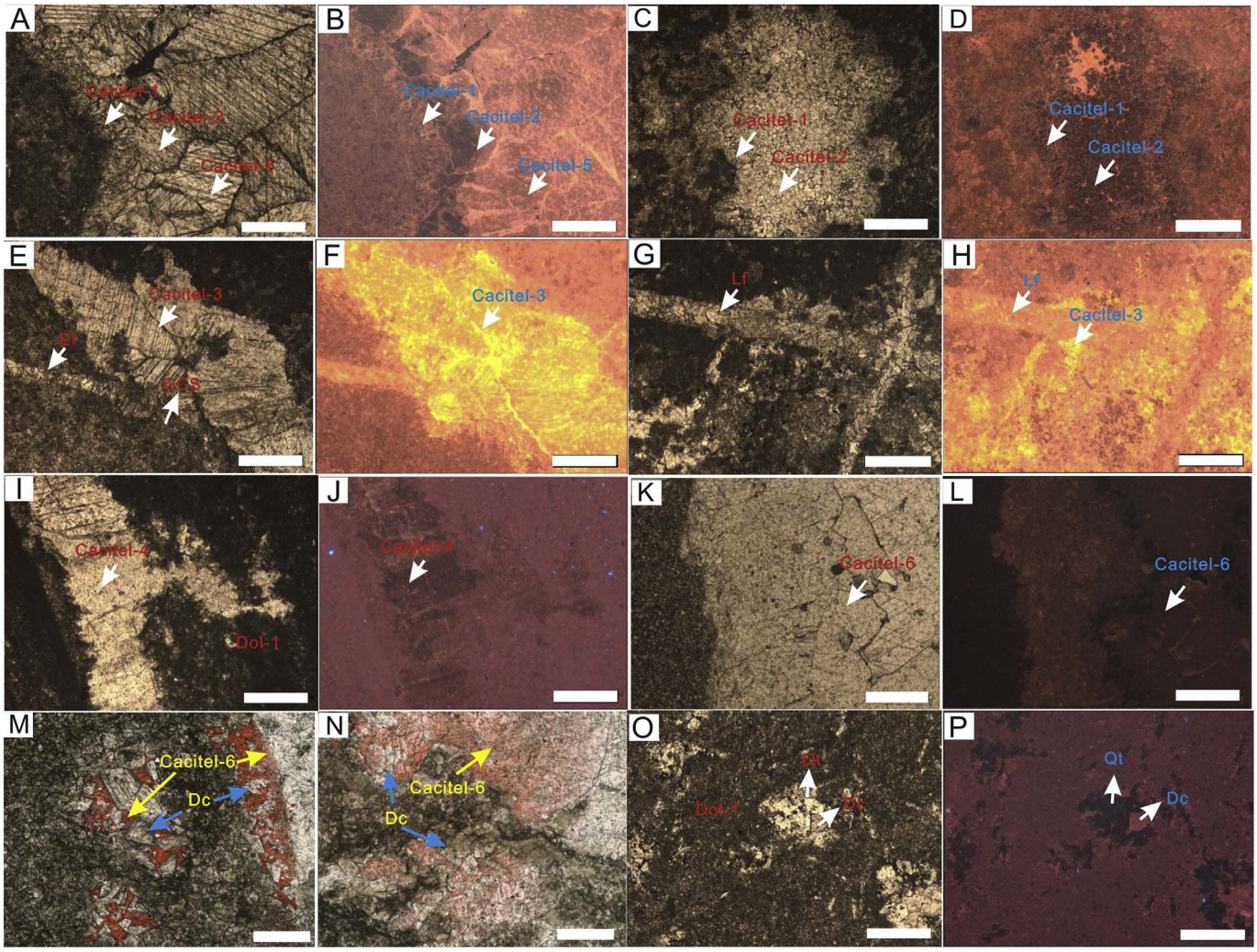

Fig. 8. Photomicrographs showing different generations of calcite cements and their cathodoluminescence features. (A)–(B) Fibrous cements with isopachous crusts (Calcite-1) and foliated cements (Calcite-2) with hackly crusts with non-luminescence. Coarse-crystalline blocky cements with weak luminescence (Calcite-5). The dark material is likely residual asphalt. (C), (D) Granular cements (Calcite-2) distributed between microbial micritic clots with non-luminescence. (E)–(H) Blocky cements (Calcite-3) with variably sized crystals and bright orange luminescence. Note two phases fractures and the early fractures (Ef) occluded by cements are cut by Calcite-3 or late fractures (Lf). (I), (J) Syntaxial cements showing clean crystal surfaces with nonluminescenc. (K), (L) Coarse-crystal cements (Calcite-6) with non-luminescence. (M), (N) Dissolved saddle dolomite remnants suspended in the Calcite-6; the red zone was stained with Alizarin red S and potassium ferricyanide. (O), (P) The authigenic quartz and dolomite cements in pores. (For interpretation of the references to colour in this figure legend, the reader is referred to the Web version of this article.)

stratified dissolution horizons that are 0.1–3 m in thickness and have a good inter-pore connectivity (Fig. 9A–E). Vuggy porosity consists of millimetre-to centimetre-sized (between 0.1 and 20 mm), irregular, dendritic to sub-angular patch pores (Figs. 5D, 6A and 9A). Caves that are centimetre-to metre-sized are irregularly elongated and sub-spherical (Fig. 9B). Some pores occluded by sparry calcite cements suggesting that a dissolution process took place prior to cementation (Figs. 6D and 9A).

Mouldic porosity is widely distributed in the intraclastic to peloidal masses, especially in the grainstone to packstone intervals of stromatolites (Fig. 5D) and dense micritic clots with dolomitization of thrombolites (Fig. 9G and H). This fabric-selective porosity affects peloids, intraclasts, dolosparite and gypsum, generating low to moderate inter-pore connectivity (Fig. 9F and G).

Fractures that are characterized by multiple episodes and fills are grouped with microbialites (Fig. 6D). Unfilled fractures provide a route for dissolution fluid and enhance the porosity and permeability of the hydrocarbon reservoir rocks (Fig. 9G). The earlier millimetre-to decimetre-sized microfractures are generally filled by sparry calcite cements, which are commonly named calcite veins. Intercrystalline and intragranular pores are commonly observed in fabric-destructive dolomites (Fig. 7A–D, 9I-L) that are wrapped by filamentous and extracellular polymeric substances (EPSs, Fig. 9K and L).

5.2. Porosity and permeability

According analyses ofconventional physical properties of microbialites (Fig. 10), the thrombolites with thrombolitic textureshave a porosity (q) and permeability (K) of 0.30%–10.63% and (0.0001–0.98425) × 10^{-3}μm^2, respectively, with averages of 3.22% and 0.12022 × 10^{-3}μm^2, respectively; Fabric-destructive dolomite (Dol-2) with microbial textures in the thrombolites has a porosity and permeability of 0.98%–12.64% and (0.0001–1.18981) × 10^{-3}μm^2, respectively, with averages of 4.52% and 0.26966 × 10^{-3}μm^2, respectively. The stromatolite has a porosity and permeability of 0.38%–14.92% and (0.0001–0.0.93674) × 10^{-3}μm^2, respectively, with an average of 3.92% and 0.15632 × 10^{-3}μm^2, respectively. The permeability is low, which may be caused by sample selection in the field (fragile samples are commonly eliminated).

Physical property tests show that the microbialite reservoirs have the following several characteristics: (1) the thrombolite (limestone and dolomitic limestone) intervals are low porosity and low permeability,

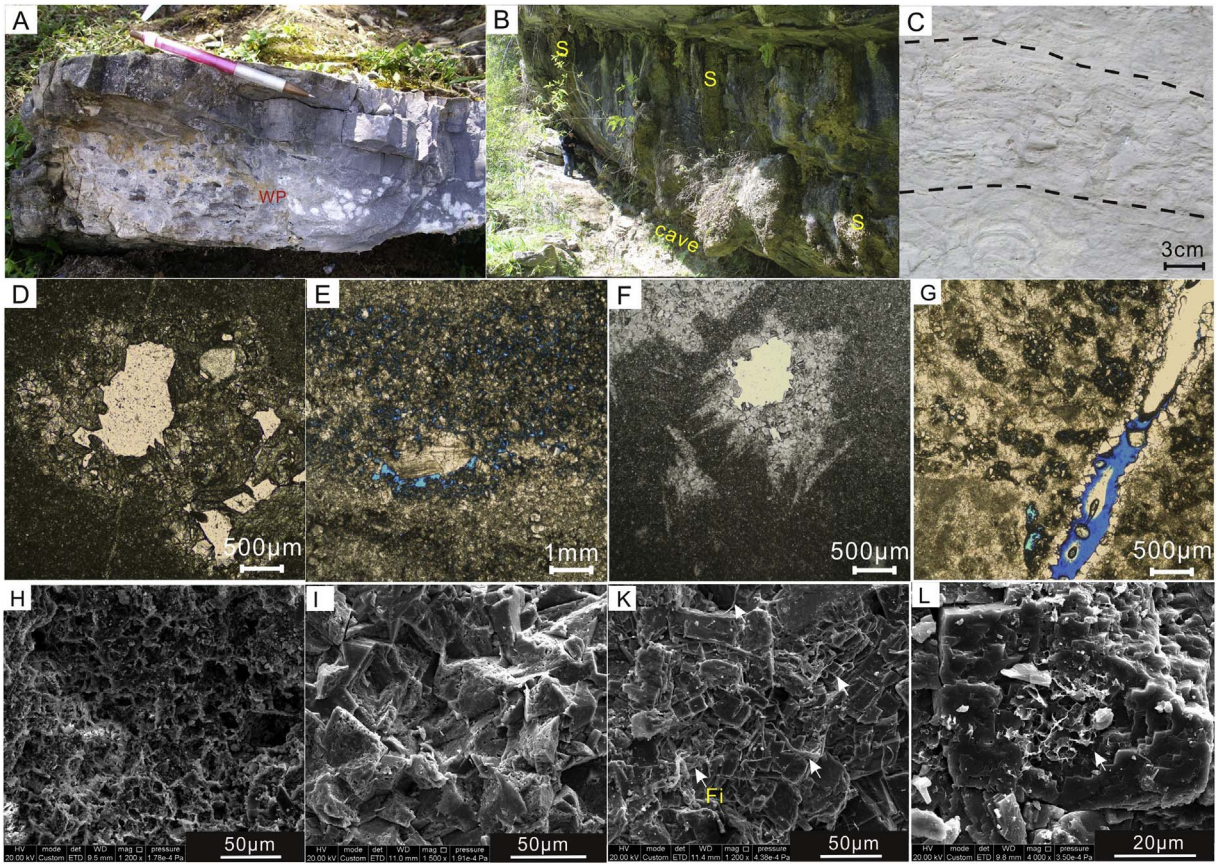

Fig. 9. Types of porosity in microbialites. (A)–(C) Macrostructure of vuggy porosity and caves showing well-stratified dissolution horizons that are 0.1–1.4 m in thickness. (A) and (C) show good inter-pore connectivity and (B) shows a cave filled by with carbonate sands, breccias and muds. Note the vertical stalactites (S) the upper part of the cave. (D) Microstructure of a cave with a sub-spherical texture. (E) Vuggy pores with good inter-pore connectivity in the Dol-2. (F) Isolated rose-shaped pore, indicating dissolved gypsum. (G) Fractures and mouldic porosity. (H) Honeycomb mouldic porosity with different sizes that developing in the Dmc. (I) Honeycomb-shaped dissolved pores in the 50 μm dolomite crystals. (K) Intercrystalline and intragranular pores. Some pores are completely occluded by microbial filaments. (L) Degradation of EPS around and in the dolomite crystal.

and are not qualified as reservoirs; (2) stromatolite reservoirs have a high heterogeneity; (3) the fabric-destructive dolomite reservoirs show high porosity and permeability with a good relationship. According to the characteristics of reservoirs in the central Sichuan Basin (where reservoirs with porosity > 2% and permeability > $0.001 \times 10^{-3}\mu m^2$ are interpreted as valid reservoirs, Tian et al., 2014; Jin et al., 2014), the microbialite units in the Qingxudong Formation can likely be regarded as potential reservoirs.

6. Geochemical characteristics

In this study, carbon/oxygen isotope analyses were performed for stromatolites, thrombolites, vug-fillings, and microcrystalline limestone (Table 2 and Fig. 11). The $\delta^{13}C_{V\text{-}PDB}$ and $\delta^{18}O_{V\text{-}PDB}$ values of

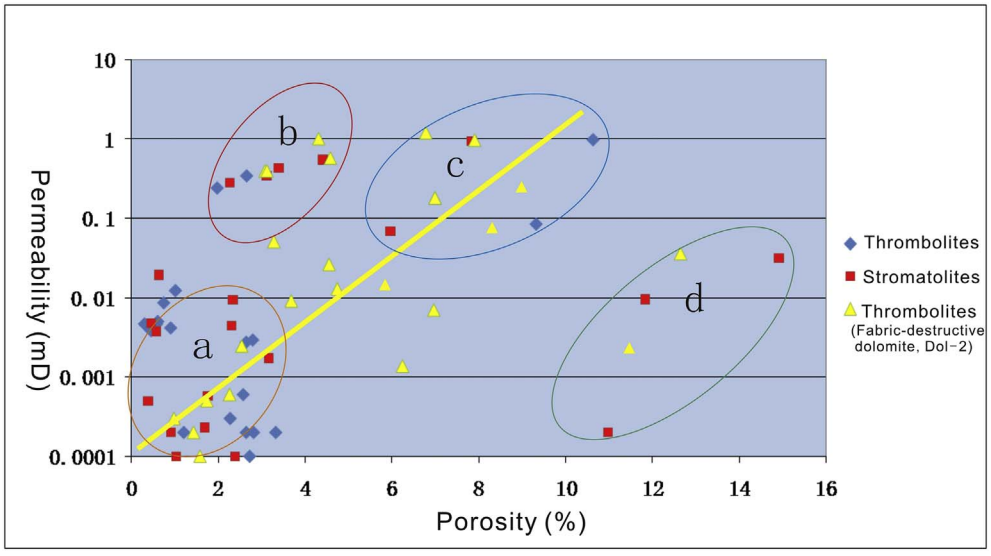

Fig. 10. Physical properties of microbialite. "a" shows the physical properties of the microbialite matrix, "b" shows the physical properties that are affected by fractures, "c" shows vuggy porosity and "d" shows caves, which is a physical property affected by dissolution.

Table 2
$\delta^{13}C$, $\delta^{18}O$, and $^{87}Sr/^{86}Sr$ values of the hole-filling calcites in microbialites of Qingxudong formation.

Types	Number of samples	Lithology	δ^{13}CPDB(‰)	δ^{18}OPDB(‰)	Z values	$^{87}Sr/^{86}Sr$ (error(2σ))
Thrombolite	YK-6-1	calcitedolomite	0.37	−8.75	123.70	–
	RX-3-1		1.25	−8.96	124.88	0.709642(9.00×10^{-5})
	YK-5-1		1.37	−7.70	126.28	0.709563(3.49×10^{-5})
	NSP-30-1	Neomorphic dolomite (Dol-2)	0.11	−7.00	124.04	0.709760(3.14×10^{-5})
	NSP-30C		−0.17	−6.32	123.79	0.709102(4.30×10^{-5})
	THC-5-1		1.17	−7.40	123.01	0.709321(6.10×10^{-5})
	THC-4-3		1.13	−7.61	124.88	0.710536(7.55×10^{-5})
Stromatolite (Dol-1)	YK-16-2	dolomite (Dol-1)	−0.37	−6.21	122.59	0.711261(3.44×10^{-5})
	YK-17-1		−0.76	−6.33	122.85	–
	YK-30-1		−1.60	−5.45	121.31	0.709875(1.35×10^{-5})
	YK-30-2		−0.63	−7.53	122.26	–
	RX-29-1		−0.58	−6.74	122.75	–
	RX-29-3		−0.44	−4.90	123.96	0.710088(6.68×10^{-5})
	THC-19-2		−1.69	−5.46	121.11	0.709973(1.33×10^{-5})
vug-fillings	YK-6-1d	calcite-5	0.65	−9.21	124.05	0.709275(2.44×10^{-5})
	THC-2d		0.56	−9.67	123.62	0.709444(2.14×10^{-5})
	THC-3d	calcite-1 and 2	0.37	−8.13	124.02	0.709547(2.87×10^{-5})
	YK-6-4d		0.84	−8.40	124.83	0.709810(1.24×10^{-5})
	YK-6-2d	calcite-3	−3.25	−8.24	116.55	0.709864(5.49×10^{-5})
	THC-5d		−3.18	−10.33	115.65	0.71265(1.05×10^{-5})
	THC-7d		−2.46	−8.60	117.98	0.710022(1.91×10^{-5})
		calcite-6	−6.03	−9.83	–	–
	[a]THC-19d		−17.37	−10.13	–	0.709973(1.33×10^{-5})
	[a]RX-29d		−29.64	−9.59	–	0.713744(6.24×10^{-5})
Micrite limestone	SL-1	micrite limestone (seawater)	0.70	−8.45	124.51	0.709647(3.27×10^{-5})
	YK-8		1.54	−8.58	126.18	0.709353(3.17×10^{-5})
	THC-3		1.70	−6.24	127.67	0.709598(8.53×10^{-6})

Notes: "—" date not measured or unavailable.

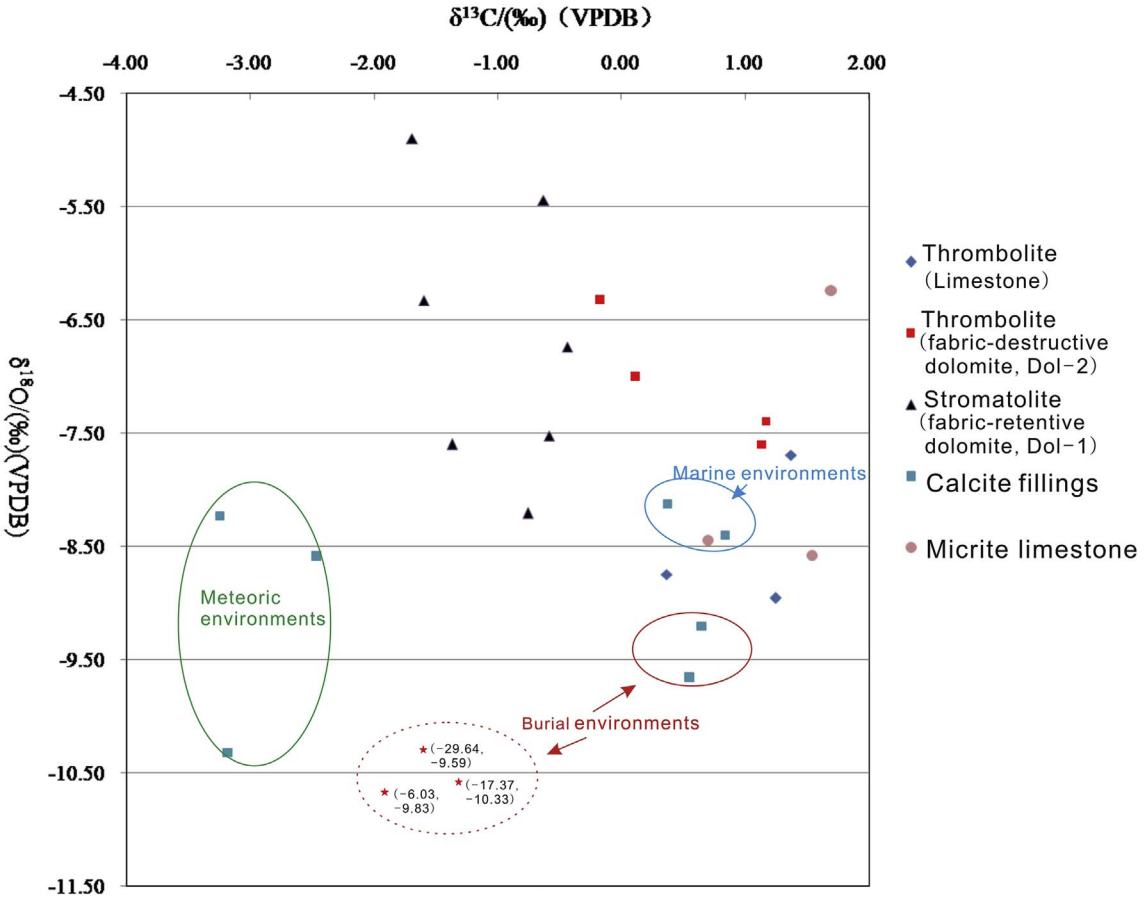

Fig. 11. Carbon and oxygen isotope characteristics of microbialites and vug-filling calcites in the lower Cambrian Qingxudong Formation.

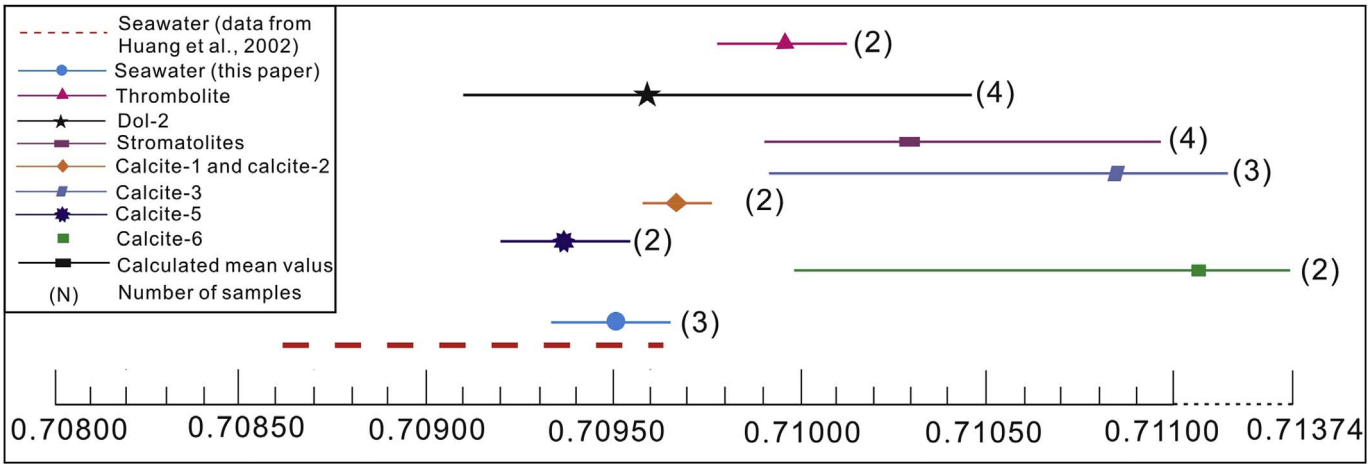

Fig. 12. Strontium isotopic ratios of microbialites and vug-filling calcites in the lower Cambrian Qingxudong Formation.

stromatolites varied from −1.69‰ to −0.37‰ (average −0.87‰) and from −7.53‰ to −6.38‰ (average −6.09‰), respectively. The $\delta^{13}C_{V\text{-}PDB}$ and $\delta^{18}O_{V\text{-}PDB}$ values of thrombolites (limestone and dolomite) varied from 0.37‰ to 1.37‰ (average 0.99‰) and from −8.96‰ to −7.70‰ (average −8.47‰), respectively. The $\delta^{13}C_{V\text{-}PDB}$ and $\delta^{18}O_{V\text{-}PDB}$ values of vug-fillings varied from −29.64‰ to 0.65‰ and from −10.33‰ to −8.24‰, respectively. The $^{87}Sr/^{86}Sr$ values of stromatolites, thrombolites and holes fillings varied from 0.709875 to 0.711262, from 0.709642 to 0.710537 and from 0.709275 to 0.713744, respectively (Fig. 12). The microcrystalline limestone samples had $^{87}Sr/^{86}Sr$ values of 0.709353–0.709353 (Table 2). Moreover, Mn/Sr values of the microcrystalline limestone samples are less than 1, indicating a negligible influence of diagenesis (Flügel, 2004). Carbon, oxygen and strontium isotopes values of seawater during the late lower Cambrian Period range from 0‰ to 2‰, from −10‰ to −5‰, and from 0.708682 to 0.709626 respectively (Huang et al., 2002; Zuo et al., 2008; Fan et al., 2011; Adachi et al., 2014; Tan et al., 2017).

7. Discussion

7.1. Relative timing of diagenetic processes

Three major diagenetic settings are identified according to petrographic and geochemical analyses, including marine, eogenetic and mesogenetic (shallow to deep burial) settings. The relative timing of the diagenetic processes is identified for the microbial reefs of Qingxudong Formation (Fig. 13).

7.1.1. Marine processes

Fibrous cements (Calcite-1), granular cements (Calcite-2), microbial crusts and microcrystalline dolomite (DOL-1) are the major diagenetic products that reveal marine diagenesis (Fig. 13). Calcite-1 and Calcite-2, which are non-luminescent in the thrombolites, are regarded as marine cementation (Flügel, 2004; Shi et al., 2013). The $\delta^{13}C$ values (0.37‰–0.84‰), $\delta^{18}O$ values (−8.13‰ to −8.40‰) and $^{87}Sr/^{86}Sr$ values (0.709547–0.709811) of Calcite-1 and Calcite-2 (Table 1, Figs. 11 and 12) are similar to those of Early Cambrian seawater, suggesting marine-phreatic and marine-vadose environments (Flügel, 2004; Shi et al., 2013). In other cases, the microbial crusts remained as a substrate for growth of fibrous cements, suggesting that a microbial micritization process took place prior to marine cementation (Fig. 6H).

Stromatolites are characterized by fabric-retentive microcrystalline dolomites (Dol-1) that are interpreted to represent a syn-sedimentary dolomitization process (Dupraz et al., 2009; Hips et al., 2015). The $\delta^{13}C$ values (−1.69‰–0.37‰, average −0.87‰, n = 7) of Dol-1 are more negative than Cambrian seawater values, but the $\delta^{18}O$ values (−7.53‰ to −6.38, average −6.09‰, n = 7) were not depleted (Table 2, Fig. 11), suggesting the microbial influences rather than the meteoric influences were involved in dolomitization (Andrews et al., 1997; Luzon et al., 2009). Degradation of EPS through microbial sulfate-reducing metabolic activities is regarded as major importance in formations of the Dol-1 (Vasconcelos and McKenzie, 1997; Perri and Tucker, 2007; Hips et al., 2015). The high $^{87}Sr/^{86}Sr$ values (average 0.710408) indicate that the Dol-1 was contaminated by clastic detritus (Fig. 12).

7.1.2. Eogenetic processes

The Cambrian tectonic history suggests that the sediments were exposed during late deposition of theQingxudong Formation (Jin et al., 2014; Zou et al., 2014; Zhou et al., 2014). Therefore, the eogenetic environment of the Qingxudong Formation may include two stages: the syn-sedimentary and near-surface stages (Fig. 13). During syn-sedimentary stage, the microbial reefs in the Qingxudong formation were exposed intermittently and locally due to sea level fluctuations. In the near-surface stage, the microbial reefs were exposed entirely and widely because a sea-level lowstand during late deposition of the Qingxudong Formation.

The syn-sedimentary stage is likely characterized by fabric-selective dissolution (Dis-1) and dolomitization due to intermittent and transitory exposure. Fenestral porosity and desiccation cracks (Fig. 5D) provided indicators of the exposure (Flügel, 2004). Most of the pores produced by Dis-1 were occluded by sparry calcite cements of marine and meteoric origin, including Calcite-1, Calcite-2 and Calcite-3, suggesting that Dis-1 formed earlier than marine and meteoric cements. The low $\delta^{13}C$ values (−2.46‰ to −3.25‰, average −2.96‰, n = 3), high $^{87}Sr/^{86}Sr$ values (0.709864–0.712654, average 0.710847, n = 3) and low Z values (115.6–117.9, according to the empirical formula) of Calcite-3 (Table 1, Figs. 11 and 12) suggest that they formed in meteoric-phreatic and/or meteoric-vadose environments (Back et al., 1986; Flügel, 2004).

The near-surface stage is marked by early fractures (Fr-1), non-fabric-selective dissolution (Dis-2) and dolomitization that occurred during steady sea-level lowstand. Most of the pores that are related to dolomitized zones that were produced by Dis-2 are not currently occluded by calcite cementation. The dolomitization of microbial reefs in the eogenetic stages is characterized by fabric-destructive dolomites (Dol-2). The $\delta^{13}C$ values (−0.17‰–1.17‰, average 0.56‰, n = 4), $\delta^{18}O$ values (−6.32‰ to −7.61‰, average −7.08‰, n = 4) and $^{87}Sr/^{86}Sr$ values (0.709102–0.710536, average 0.709680, n = 4) are consistent with original marine values, suggesting that the dolomitization of Dol-2 was mediated by seawater or slightly modified seawater. Dolomitization of the Calcite-1 and Calcite-2 resulted in Dol-2 suggests that dolomitization post-dated the cement precipitation. Early fractures

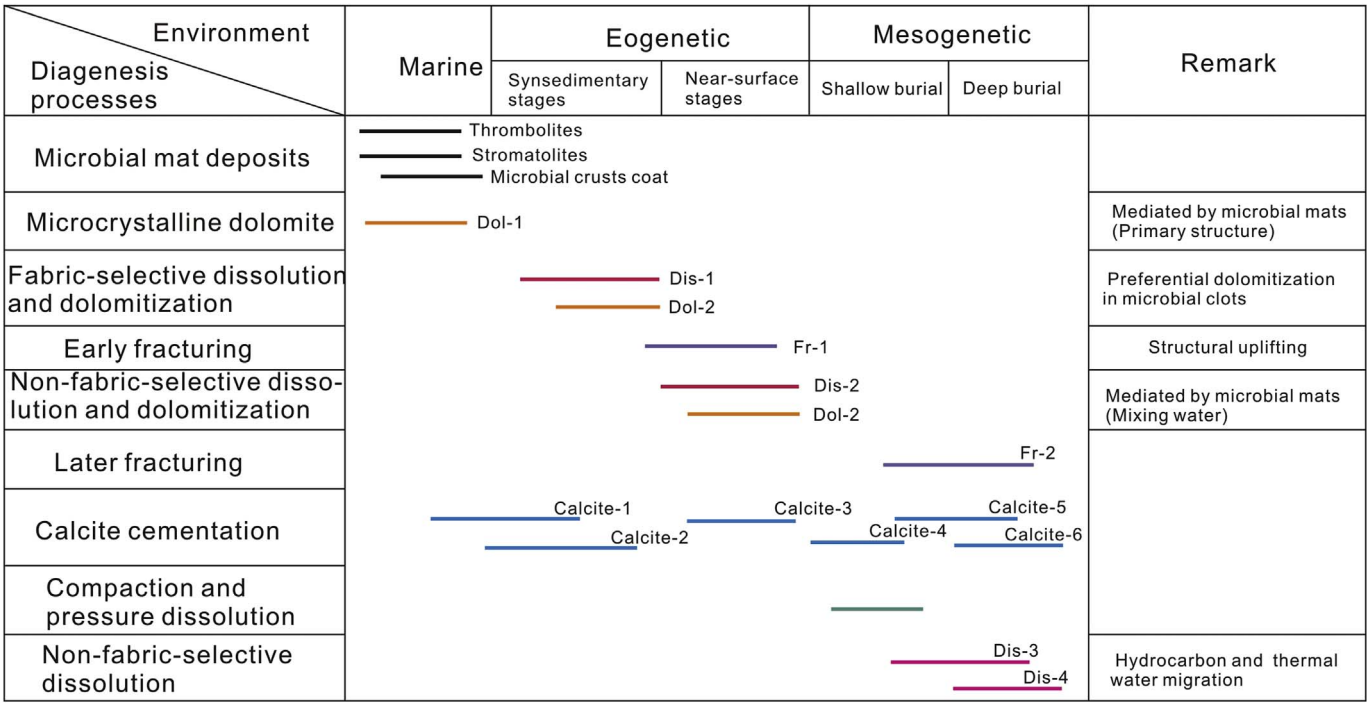

Fig. 13. Paragenetic sequence of the Qingxudong Formation in southeastern Sichuan Basin.

are currently cut by pores filled with cements, suggesting that Fr-1 occurred prior to Dis-2.

7.1.3. Mesogenetic processes

In the shallow and middle burial diagenesis stages, a series of diagenetic processes occurred (Fig. 13). Compaction increased with increased of burial depth, resulting in the precipitation of Calcite-5 with $\delta^{18}O$ values of −9.21‰ to −9.67‰ due to the increase of carbonate saturation and development of stylolites associated with pressure dissolution (Dis-3). Subsequently, the oil and gas charged, resulting in the precipitation of dolomite cements (coarse and saddle dolomites), authigenic quartz and a second stage of fracturing (Fr-2).

In deep burial diagenesis stage, the fourth stage of dissolution (Dis-4) and the precipitation of Calcite-6 occurred. Calcite-6 with low $\delta^{13}C$ values of −29.64‰ to −6.03‰ and a large concentration of pyrites in the Dol-1 and Dol-2 suggest that the calcite was induced by thermal sulfate reduction (TSR, Machel, 2001; Zhu et al., 2006; Jia et al., 2015).

7.2. Porosity origin and evolution of microbialite

7.2.1. Porosity origin and evolution of stromatolites

The formation of stromatolites with many original pores (fenestral pores and interlaminar voids) is related to microbial metabolic activities (Riding, 2000; Mercedes-Martín et al., 2014) that can induce the deposition of aragonite, high Mg-calcite and dolomite (Fig. 5F, Hover, et al., 2001; Visscher and Stolz, 2005; Brauchli et al., 2016). Stromatolites formed in a low-energy tidal flat environment with high evaporation, suggesting that original pores may have originated during desiccation and dewatering in hot conditions. The original pores were enlarged by subsequent dissolution processes to become vuggy pores (Fig. 5H). However, the original pores are currently occluded by cements later.

In the syn-sedimentary stage, selective dissolution (Dis-1) of dissolvable mineral (e.g. aragonite, high Mg-calcite and gypsum) produced a large number of mouldic pores and vuggy pores during subaerial exposure of stromatolites (Fig. 5D–F and 8F, H). Dissolution (Dis-1) began in the original pores and the pores were later partly occluded by marine cementation (Calcite-1 and/or Calcite-4), suggesting that dissolutions occurred contemporaneously with marine cementation or prior to marine cementation. Meteoric cementation (Calcite-3) occluded pores, suggesting meteoric dissolution involved in porosity creation. Moreover, Bacterial sulfate reduction (BSR) that was involved in stromatolite formation would create acidic fluid that is rich in H_2S and CO_2 that may be beneficial for dissolvable mineral dissolution.

Following the increase in burial depth, especially during the early Permian, tectonic and magmatic activity drive drove upward hydrothermal fluid flow through high-permeability faults and fractures (Shi et al., 2013; Zhang et al., 2017). The presence of authigenic quartz (Fig. 9O, P) implies that the hydrothermal fluids were acidic (Li et al., 2016), suggesting that the hydrothermal fluids could lead to corrosion and enhance porosity. Some authors had emphasized that TSR related to hydrothermal fluids had an overall destructive effect on reservoirs quality (Hao et al., 2015; Zhang et al., 2017), however, TSR dissolution has been observed in stromatolites (Fig. 9A). Two types of TSR calcites are identified in stromatolites (Fig. 9A), one (Calcite-6-1) characterized by −6.03‰ of $\delta^{13}C$ values (left of Fig. 9A) was partly occluded the porosity and the other (Calcite-6-2) characterized by −17.37‰ of $\delta^{13}C$ values (right of Fig. 9A) was completely occluded the porosity. The porosity was partly occluded by Calcite-6-1 has a significant enlargement (Fig. 9A), suggesting the TSR involved in Dol-1 dissolution through reaction 1 (R1, $CaMg(CO_3)_2 + SO_4^{2-} + 2CH_4 + 2H^+ \rightarrow Mg^{2+} + CaCO_3$ (Calcite-6-1) $+ 2HCO_3^- + H_2S + CO_2 + 3H_2O$, Cai et al., 2014) and R2 ($CaMg(CO_3)_2 + 4H^+ \rightarrow Mg^{2+} + Ca^{2+} + 2CO_2$ (^{13}C-rich) $+ 2H_2O$). However, the TSR Calcite-6-2 occluded the porosity through R3 (Liquid hydrocarbons $+ SO_4^{2-} \rightarrow$ Organosulfur compounds + solid bitumen $+ H_2S + CO_2$ (^{12}C-rich), Hao et al., 2015) and R4 ($Ca^{2+} + CO_2$ (^{12}C-rich) $+ H_2O \rightarrow CaCO_3 + 2H^+$, Hao et al., 2015). The dolomite with ^{13}C-rich was involved calcite (Calcite-6-1) precipitation, resulting in higher $\delta^{13}C$ values. The Calcite-6-2 with ^{13}C depleted is related to ^{12}C-rich CO_2 generated by hydrocarbons react with sulfate.

7.2.2. Porosity origin and evolution of thrombolites

There is significant difference in porosity evolution between stromatolites and thrombolites. The thrombolites with shelter porosity (original pores) are commonly considered to form in a low-to mild-

energy subtidal environment that is unfavourable for intermittent meteoric diagenesis. Furthermore, lack of remnants of calcrete components (such as desiccation cracks and pendant cement) also suggests that Dis-1 contributed little to the development of porosity during synsedimentary stage.

When thrombolites were exposed to the surface during sea-level lowstand in the near-surface stage, the dissolvable minerals were dissolved by vadose and phreatic fresh water, which created vuggy pores and enlarged pores. These pores were commonly filled by subsequent calcite cements. However, most vuggy pores, enlarged pores and caves formed near the halocline and not currently occluded by cement in this stage. Mixed freshwater and seawater were historically regarded as the important fluids in the dissolution and dolomitizing processes (Back et al., 1986; Flügel, 2004; Mylroie and Mylroie, 2007). However, the geochemical characteristics of the fabric-destructive dolomites (Dol-2) suggest that the Dol-2 was commonly mediated by normal seawater or slightly modified seawater, not mixed water. Furthermore, vertical stalactites widely distributed in the top of caves, suggesting the vadose fluid in the top of mixing zones are supersaturated with $CaCO_3$, and thus are not conducive for dissolution.

Microbial communities with complex biogeochemical processes have been shown to significantly facilitate carbonate dissolution and deposition (Machel, 2001; Visscher and Stolz, 2005; Wilhartitz et al., 2009). SEM analyses show that microbial mats were involved in dolomite formation (Fig. 7). The microbial mat deposits contain abundant organic matter that can be converted to nutritive materials that are required by a microbial community. Nutritive materials that were dissolved in water likely collected near and under the halocline through high permeability and dynamic pore-fluid circulation (Fig. 14, Wilhartitz et al., 2009). The bacterial sulfate reduction (BSR, $CH_2O + SO_4^{2-} \rightarrow HCO_3^- + HS^- + H_2O$) would create high $CaCO_3$ supersaturation and alkaline conditions that be able to promote dolomitization in the marine environments (Perri and Tucker, 2007). In addition, H_2S and CO_2 were created by BSR (Visscher and Stolz, 2005) dissolved in surrounding water. The acidic fluids were discharged from the flanks of microbial reefs and thus the vuggy porosity and flank-margin caves formed (Fig. 14B). Accordingly, organic matter, sea level and microbial communities were the most important controlling factors of dissolution and dolomitizing in microbial reefs. Pores that occurred in microbial limestone (diagenesis in freshwater) were filled by calcite cements and pores that occurred in fabric-destructive dolomites were not occluded by cement, suggesting that dolomitizing prevented the formation of cement and thus was favorable for the preservation of porosity.

In mesogenetic diagenesis settings, the hydrothermal fluids only resulted in the dissolution of microbial limestone along faults and fractures, because low permeability and low porosity of microbial limestone did not allow hydrothermal fluids to flow in the limestone. The porous fabric-destructive dolomites have a post-oil-charge and post-saddle dolomite-formation dissolution (Fig. 9M, N), suggesting TSR dissolution indeed occurred in diagenesis history. However, the porosity in fabric-destructive dolomites was lost by TSR Calcite-6-2, pyrite and solid bitumen precipitation through R2, R3 and R4 ($Fe^{2+} + 2H_2S \rightarrow FeS_2 + 4H^+$). No volumetrically significant pores that were partly occluded by Calcite-6-1 and volumetrically significant pores were completely occluded by Calcite-6-2 were observed in fabric-destructive dolomites, suggesting TSR has more destructive effect.

7.3. The model forthe development of microbial carbonate reservoirs

Based on the paragenetic sequence of the Qingxudong Formation in the southeastern Sichuan Basin and the analysis of the origin of porosity and the evolution of microbialites, a microbialite reservoir development model was established (Fig. 14). It includes three stages of porosity formation.

In the syn-sedimentary diagenesis stage, the stromatolites with fenestral porosity grew in low-energy tidal environments and thrombolites with shelter porosity formed in mild-energy subtidal environments. When the microbial deposits (especially stromatolites) were intermittently and transiently exposed, meteoric dissolution (Dis-1) occurred and created some fabric-selective pores (e.g. moldic and vuggy pores). However, these pores were later occluded by marine and meteoric cements. Dis-1 makes a great contribution to the dissolution of dissolvable mineral.

In the near-surface diagenesis stage (late stage of the Qingxudong formation), the microbial deposits were exposed for prolonged times when microbial seawater dissolution (Dis-2) occurred. This resulted in a large number of non-fabric-selective pores. These pores were not currently occluded by later cements and were overprinted by secondary dolomite intercrystalline and vuggy porosity in fabric-destructive dolomites. The fabric-destructive dolomites have low porosity and permeability without the dissolution, suggesting dolomitization is unfavourable for porosity enhancement but is favorable for porosity preservation. Dis-2 makes a remarkable contribution to the dissolution of limestone and fractures and faults are favorable for dissolution. Dis-1 and Dis-2 and associated fracturing are the fundamental control factors of porosity creation in microbial carbonate of the Qingxudong Formation.

In mesogenetic diagenesis settings, TSR calcites (Calcite-6 and Calcite-7) were distributed in the microbial deposits, suggesting that the TSR was involved in this part of the diagenesis history. The TSR is a double-edged sword for porosity development. TSR with Calcite-6-1 precipitate (constructive effect) is favorable for porosity enhancement in microbial dolomite. However, TSR with Calcite-6-2 precipitate (destructive effect) is unfavourable for microbialite reservoir quality. According to thin section and geochemistry analysis, the destructive effect of TSR on microbial carbonate reservoirs was more noticeable in the Qingxudong Formatio.

7.4. Implications

With the depletion of conventional oil and gas resources, deep reservoirs that are commonly characterized by microbial carbonate rocks are gradually becoming primary exploration targets worldwide, especially in China. The discovery of deeply buried microbial carbonate reservoirs in the Upper Sinian Dengying Formation in the Sichuan Basin of SW China (Shi et al., 2013), in the upper part of the Lower Cambrian Xiaoerbulake Formation in Tarim Basin of SW China (Song et al., 2014), the Upper Jurassic Smackover Formation in the Gulf of Mexico (Mancini et al., 2013), and Ediacaran–Cambrian Ara Group in the Sultanate of Oman (Grotzinger and Al-Rawahi, 2014) highlights the possibility of hydrocarbon exploration in deep microbial carbonate rocks in this basin and elsewhere. Recently, the lower Cambrian Qingxudong (Longwanmiao) Formation in the central Sichuan Basin has hosted great achievements for hydrocarbon exploration (Jin et al., 2014; Zou et al., 2014), showing great petroleum geologic conditions in the Qingxudong Formation. The original pores of microbial carbonate rocks in Qingxudong Formation have been tightly cemented, but the porosity and permeability had been improved by diagenesis. The physical properties of microbial dolomites, especially the fabric-destructive dolomites in thrombolites in the study area are similar to fabric-destructive dolomite reservoirs in centre Sichuan Basin. Therefore, the Cambrian microbial carbonate may have a great potential for gas exploration.

8. Conclusions

(1) The Qingxudong Formation microbial carbonate represents a rapid response of microbes after archaeocyathids died out. Stromatolites are characterized by fabric-retentive microcrystalline dolomites. The thrombolites were originally composed of dense microbial packstone and wackestone. Subsequently, thrombolites were partly

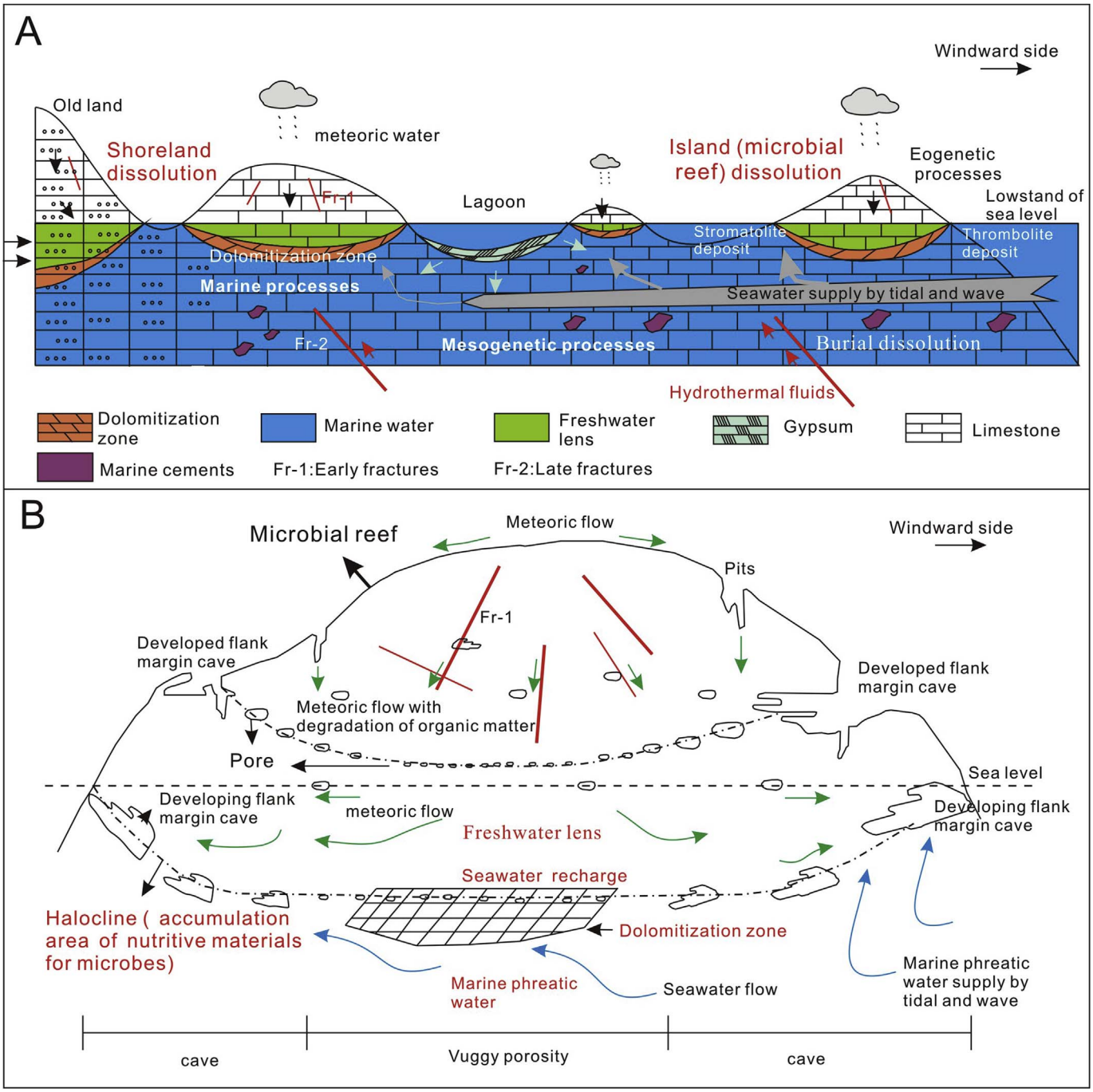

Fig. 14. (A) The development model for microbialite reservoirs in the Qingxudong Formation in the Sichuan Basin, including syn-depositional, eogenetic and mesogenetic processes. (B) The dissolution model of microbial reef in eogenetic processes.

dolomitized, and the resulting dolomites are characterized by fabric-destructive textures. Fenestral porosity, shelter porosity, mouldic porosity, vuggy porosity, caves and fractures are the major pore types in the microbial carbonate rocks observed in this study.

(2) Six stages of calcite cementation (Calcite-1 to Calcite-6) and four stages of dissolution (Dis-1 to Dis-4) were determined from petrologic features, porosity types and geochemical characteristics. Fabric-selective dissolution (Dis-1) and marine and meteoric cementations (Calcite-1, Calcite-2 and Calcite-3) currently occurred during the syn-sedimentary stage. Non-fabric-selective dissolution (Dis-2) and marine cementation (Calcite-4) formed in near-surface stage. The pressure dissolution (Dis-3), TSR dissolution (Dis-4), buried cementation (Calcite-5) and TSR calcites (Calcite-6) occurred during mesogenetic processes.

(3) Stromatolites and thrombolites show different evolution histories for porosity. The fundamental control factors of pore creation are syn-sedimentary processes in stromatolites; however, pores of thrombolite are created by dissolution and dolomitizing in the near-surface stage. Microbial metabolic activities, likely drive dissolution and dolomitization in marine phreatic conditions, but near the halocline. The thermochemical sulfate reduction (TSR) was a double-edged sword for porosity development in the Qingxudong Formation. The destructive effect of TSR played a more active role in microbial carbonate reservoirs.

Acknowledgments

This work was supported by Sinopec Exploration and Production Research Institute and National Natural Science Foundation of China (Grant No. 40739903). Dr. Jinyong Xu and Di Yang of Chengdu University of Technology helped in measuring isotope ratios of marine carbonates. Dr. Xiaoxing Gong and Prof. Haiqin Tian of Sinopec Exploration and Production Research Institute helped us in sampling collection in the field. The authors greatly appreciated all those mentioned above.

References

Adachi, N., Ezaki, Y., Liu, J.B., 2014. The late early Cambrian microbial reefs immediately after the demise of archaeocyathan reefs, Hunan Province, South China. Palaeogeogr. Palaeocl 407, 45–55.
Al Haddad, S., Mancini, E.A., 2013. Reservoir characterization, modeling, and evaluation of Upper Jurassic Smackover microbial carbonate and associated facies in Little Cedar Creek field, southwest Alabama, eastern Gulf coastal plain of the United States. AAPG Bull. 97 (11), 2059–2083.
Aloisi, G., 2008. The calcium carbonate saturation state in cyanobacterial mats throughout Earth's history. Geochim. Cosmochim. Ac 72 (24), 6037–6060.
Andrews, J.E., Riding, R., Dennis, P.F., 1997. The stable isotope record of environmental and climatic signals in modern terrestrial microbial carbonates from Europe. Palaeogeogr. Palaeocl. 129, 171–189.
Back, W., Hanshaw, B.B., Herman, J.S., Van Driel, J.N., 1986. Differential dissolution of a Pleistocene reef in the groundwater mixing zone of coastal Yucatan, Mexico. Geology 14 (2), 137–140.
Brauchli, M., McKenzie, J.A., Strohmenger, C.J., Sadooni, F., Vasconcelos, C., Bontognali, T.R.R., 2016. The importance of microbial mats for dolomite formation in the Dohat Faishakh sabkha, Qatar. Carbonates Evaporites 31 (3), 339–345.
Cai, C.F., He, W.X., Jiang, L., Li, K.K., Xiang, L., Jia, L.Q., 2014. Petrological and geochemical constraints on porosity difference between Lower Triassic sour- and sweet-gas carbonate reservoirs in the Sichuan Basin. Mar. Petrol. Geol. 56, 34–50.
Bontognali, T.R.R., Vasconcelos, C., Warthmann, R.J., Bernasconi, S.M., Dupraz, C., Strohmenger, C.J., McKenzie, J.A., 2010. Dolomite formation within microbial mats in the coastal sabkha of Abu Dhabi (United Arab Emirates). Sedimentology 57 (3), 824–844.
Dupraz, C., Reid, P.R., Braissant, O., Decho, A.W., Norman, R.S., Visscher, P.T., 2009. Processes of carbonate precipitation in modern microbial mats. Earth-Sci. Rev. 96 (3), 141–162.
Ehrenberg, S.N., Walderhaug, O., Bjorlykke, K., 2012. Carbonate porosity creation by mesogenetic dissolution: reality or illusion? AAPG Bull. 96 (2), 217–233.
Esteban, M., Taberner, C., 2003. Secondary porosity development during late burial in carbonate reservoirs as a result of mixing and/or cooling of brines. J. Geochem. Explor. 78 (1), 355–359.
Fan, R., Deng, S.H., Zhang, X.L., 2011. Significant carbon isotope excursions in the Cambrian and their implications for global correlations. Sci. China Earth Sci. 54 (11), 1686–1695.
Flügel, L.E., 2004. Microfacies of Carbonate Rocks: Analysis, Interpretation and Application. Springer-Verlag, Berlin, pp. 142–151.
Grotzinger, J., Al-Rawahi, Z., 2014. Depositional facies and platform architecture of microbialite-dominated carbonate reservoirs, Ediacaran–Cambrian Ara Group, Sultanate of Oman. AAPG Bull. 98 (8), 1453–1494.
Gulley, J.D., Martin, J.B., Moore, P.J., 2014. Vadose CO_2 gas drives dissolution at water tables in eogenetic karst aquifers more than mixing dissolution. Earth Surf. Process. Landforms 39 (13), 1833–1846.
Gulley, J.D., Martin, J.B., Moore, P.J., Murphy, J., 2013. Formation of phreatic caves in an eogenetic karst aquifer by CO_2 enrichment at lower water tables and subsequent flooding by sea level rise. Earth Surf. Process. Landforms 38 (11), 1210–1224.
Hao, F., Zhang, X.F., Wang, C.W., Li, P.P., Guo, T.L., Zou, H.Y., et al., 2015. The fate of CO_2 derived from thermochemical sulfate reduction (TSR) and effect of TSR on carbonate porosity and permeability, Sichuan Basin, China. Earth-Sci. Rev. 141, 154–177.
Hicks, M., Rowland, S.M., 2009. Early Cambrian microbial reefs, archaeocyathan interreef communities, and associated facies of the Yangtze Platform. Palaeogeogr. Palaeocl. 281 (1–2), 137–153.
Hips, K., Haas, J., Poros, Z., Kele, S., Budai, T., 2015. Dolomitization of Triassic microbial mat deposits (Hungary): origin of microcrystalline dolomite. Sediment. Geol. 318, 113–129.
Hover, V.C., Walter, L.M., Peacor, D.R., 2001. Early marine diagenesis of biogenic aragonite and Mg-calcite: new constraints from high-resolution STEM and AEM analyses of modern platform carbonates. Chem. Geol. 175 (3), 221–248.
Huang, S.J., Shi, H., Mao, X.D., Zhang, M., Sheng, M., Shen, L.C., Wu, W.H., 2002. Evolution of Sr isotopes of the Cambrian sections in Xiushan, Chongqing, and related global correlation. Geol. Rev. 48, 509–516.
Jia, L.Q., Cai, C.F., Yang, H.J., Li, H.X., Wang, T.K., Zhang, B.S., Jiang, L., Tao, X.W., 2015. Thermochemical and bacterial sulfate reduction in the Cambrian and Lower Ordovician carbonates in the Tazhong area, Tarim Basin, NW China: evidence from fluid inclusions, C, S and Sr isotopic data. Geofluids 15 (3), 421–437.
Jin, D.M., Zeng, W., Tan, X.C., Li, L., Li, Z.Y., Luo, B., Zhang, J.L., Liu, J.W., 2014. Characteristics and controlling factors of beach-controlled karst reservoirs in cambrian longwangmiao formation, moxi-gaoshiti area, Sichuan Basin, NW China. Petrol. Explor. Dev. 41 (6), 712–723.
Lambert, L., Durlet, C., Loreau, J.P., Marnier, G., 2006. Burial dissolution of micrite in Middle East carbonate reservoirs (JurassiceCretaceous): keys for recognition and timing. Mar. Petrol. Geol. 23 (1), 79–92.
Li, Q., Jiang, Z.X., Hu, W.X., You, X.L., Hao, G.L., Zhang, J.T., Wang, X.L., 2016. Origin of dolomites in the lower cambrian xiaoerbulak formation in the Tarim Basin, NW China: implications for porosity development. J. Asian Earth Sci. 115, 557–570.
Li, W., Yu, H.Q., Deng, H.B., 2012. Stratigraphic division and correlation and sedimentary characteristics of the Cambrian in central southern Sichuan Basin. Petrol. Explor. Dev. 39 (6), 725–735.
Luzon, A., Mayayo, M.J., Perez, A., 2009. Stable isotope characterization of co-existing carbonates from the Holocene Gallocanta lake (NE Spain): palaeolimnological implications. Int. J. Earth Sci. 98 (5), 1129–1150.
Mancini, E.A., Morgan, W.A., Harris, P.W., Parcell, W.C., 2013. Introduction: AAPG Hedberg research conference on microbial carbonate reservoir characterization—conference summary and selected papers. AAPG Bull. 97 (11), 1835–1847.
Mei, M.X., Zhang, H., Meng, X.Q., Chen, Y.H., 2006. Sequence-stratigraphic frameworks and their forming backgrounds of paleogeography for the lower cambrian of the upper-yangtze region. Geoscience 33, 1292–1304.
Menning, D.M., Wynn, J.G., Garey, J.R., 2015. Karst estuaries are governed by interactions between inland hydrological conditions and sea level. J. Hydrol. 527, 718–733.
Mercedes-Martín, R., Arenas, C., Salas, R., 2014. Diversity and factors controlling widespread occurrence of syn-rift Ladinian microbialites in the western Tethys (Triassic Catalan Basin, NE Spain). Sediment. Geol. 313, 68–90.
Machel, H.G., 2001. Bacterial and thermochemical sulfate reduction in diagenetic settings – old and new insights. Sediment. Geol. 140 (1–2), 143–175.
Mylroie, J.R., Mylroie, J.E., 2007. Development of the carbonate island karst model. J. Cave Karst Stud. 69 (1), 59–75.
Pederson, C.L., Mcneill, D.F., Klaus, J.S., Swart, P.K., 2015. Deposition and diagenesis of marine oncoids: implications for development of carbonate porosity. J. Sediment. Res. 85 (11), 1323–1333.
Perri, E., Tucker, M., 2007. Bacterial fossils and microbial dolomite in Triassic stromatolites. Geology 35 (3), 207–210.
Parcell, W.C., 2002. Sequence stratigraphic controls on the development of microbial fabrics and growth forms—Implications for reservoir quality in the Upper Jurassic (Oxfordian) Smackover Formation, Eastern Gulf Coast, U.S.A. Carbonates Evaporites 17 (2), 166–181.
Raeisi, E., Mylroie, J.E., 1995. Hydrodynamic behavior of caves formed in the fresh-water lens of carbonate islands. Carbonates Evaporites 10 (2), 207–214.
Ren, Y., Zhong, D.K., Gao, C.L., Yang, X.Q., Xie, R., Li, Z.P., Deng, M.X., Zhou, Y.C., 2016. Geochemical characteristics, genesis and hydrocarbon significance of dolomite in the Cambrian Longwangmiao Formation, Eastern Sichuan Basin. Acta Pet. Sin. 37 (8), 1–14.
Rezende, M.F., Tonietto, S.N., Pope, M.C., 2013. Three-dimensional pore connectivity evaluation in a Holocene and Jurassic microbialite buildup. AAPG Bull. 97 (11), 2085–2101.
Riding, R., 2000. Microbial carbonates: the geological record of calcified bacterial–algal mats and biofilms. Sedimentology 47 (Suppl. 1), 179–214.
Scotese, C.R., 2001. Atlas of Earth History. Paleogeography. PALEOMAP Project 1, Arlington, Texas.
Shi, Z.J., Wang, Y., Tian, Y.M., Wang, C.C., 2013. Cementation and diagenetic fluid of algal dolomites in the Sinian Dengying Formation in southeastern Sichuan Basin. Sci. China Earth Sci. 56 (2), 192–202.
Shiraishi, F., Reimer, A., Bissett, A., de Beer, D., Arp, G., 2008. Microbial effects on biofilm calcification, ambient water chemistry and stable isotope records in a highly supersaturated setting (Westerhfer Bach, Germany). Palaeogeogr. Palaeocl. 262 (1–2), 91–106.
Słowakiewicz, M., Tucker, M.E., Pancost, R.D., Perri, E., Mawson, M., 2013. Upper Permian (Zechstein) microbialites: Supratidal through deep subtidal deposition, source rock, and reservoir potential. AAPG Bull. 97 (11), 1921–1936.
Song, J.M., Luo, P., Yang, S.S., Yang, D., Zhou, C.M., Li, P.W., Zhai, X.F., 2014. Reservoirs of Lower Cambrian microbial carbonates, TarimBasin, NW China. Petrol. Explor. Dev. 41 (4), 404–414.
Steiner, M., Zhu, M., Zhao, Y., Erdtmann, B., 2005. Lower Cambrian Burgess Shale-type fossil associations of South China. Palaeogeogr. Palaeocl 220 (1), 129–152.
Tian, Y.H., Liu, S.G., Zhao, Y.H., Song, J.M., Sun, W., Liang, F., Zhang, C.J., Li, J.L., 2014. Diagenesis of Lower Cambrian Longwangmiao Formation reservoirs in central area of Sichuan Basin, China. J. Chengdu Univ. Technol. 41 (6), 671–683.
Tan, Q., Shi, Z.j., Tian, Y.M., Wang, Y., Wang, C.C., 2017. Origin of ooids in ooidal-muddy laminites: A case study of the lower Cambrian Qingxudong Formation in the Sichuan Basin, South China. Geol. J. 1–12. https://doi.org/10.1002/gj.2995.
Vasconcelos, C., McKenzie, J.A., 1997. Microbial mediation of modern dolomite precipitation and diagenesis under anoxic conditions, Lagoa Vermelha, Rio de Janeiro, Brazil. J. Sediment. Res. 67 (3), 378–390.
Vacher, H.L., Mylroie, J.E., 2002. Eogenetic karst from the perspective of an equivalent porous medium. Carbonates Evaporites 17 (2), 182–196.
Visscher, P.T., Stolz, J.F., 2005. Microbial mats as bioreactors: populations, processes and products. Palaeogeogr. Palaeocl. 219 (1), 87–100.
Wilhartitz, I.C., Kirschner, A.K.T., Stadler, H., Herndl, G.J., Dietzel, M., Latal, C., Mach, R.L., Farnleitner, A.H., 2009. Heterotrophic prokaryotic production in ultra-oligotrophic alpine karst aquifers and ecological implications. FEMS Microbiol. Ecol. 68 (3), 287–299.
Yang, X.F., Wang, X.Z., Yang, Y.M., Li, X.Y., Jiang, N., Xie, J.R., Luo, W.J., 2015. Diagenesis of the dolomite reservoir in the Lower Cambrian Longwangmiao Formation in Central Sichuan Basin. Geol. Sci. Technol. Inf. 34 (1), 35–41.

Zhang, H., Cai, Z.X., Qi, L.X., Yun, L., 2017. Diagenesis and origin of porosity formation of Upper Ordovician carbonate reservoir in northwestern Tazhong condensate field. J. Nat. Gas Sci. Eng. 38, 139–158.
Zhou, J.G., Xu, C.C., Yao, G.S., Yang, G., Zhang, J.Y., Hao, Y., et al., 2014. Genesis and evolution of Lower Cambrian Longwangmiao Formation reservoirs, Sichuan Basin, SW China. Petrol. Explor. Dev. 42 (2), 175–184.
Zhu, Y.G., Zhang, Y.C., Liang, Y.B., Ma, Y.S., Dai, J.X., Zhou, G.Y., 2006. Dissolution and alteration of the deep carbonate reservoirs by TSR. An important type of deep-buried high-quality carbonate reservoirs in Sichuan basin. Acta Petrolo. Sin 22, 2182–2194.
Zou, C.N., Du, J.H., Xu, J., Wang, Z.C., Zhang, B.M., Qi, W.G., Wang, T.S., Yao, G.S., Deng, S.W., Liu, J.J., 2014. Formation, distribution, resource potential and the discovery of Sinian-Cambrian giant gas field, Sichuan Basin, SW China. Petrol. Explor. Dev. 41 (3), 278–293.
Zuo, J.Z., Peng, S.C., Zhu, X.J., 2008. Carbon isotope composition of Cambrian carbonate rocks in Yangtze Platform, South China and its geological implication. Geochimica 37, 118–128.